

A new suite of Lund-tree observables to resolve jets

Melissa van Beekveld,^a Luca Buonocore,^b Silvia Ferrario Ravasio,^{b,c} Pier Francesco Monni,^b Alba Soto-Ontoso,^d Gregory Soyez^e

^a*Nikhef, Theory Group, Science Park 105, 1098 XG, Amsterdam, The Netherlands*

^b*CERN, Theoretical Physics Department, CH-1211 Geneva 23, Switzerland*

^c*Dipartimento di Fisica, Università di Torino, and INFN, Sezione di Torino, Via P. Giuria 1, I-10125 Torino, Italy*

^d*Departamento de Física Teórica y del Cosmos, Universidad de Granada, Campus de Fuentenueva, E-18071 Granada, Spain*

^e*IPhT, Université Paris-Saclay, CNRS UMR 3681, CEA Saclay, F-91191 Gif-sur-Yvette, France*

E-mail: mbeekvel@nikhef.nl, luca.buonocore@cern.ch,
silvia.ferrari.ravasio@unito.it, aontoso@ugr.es, pier.monni@cern.ch,
gregory.soyez@ipht.fr

ABSTRACT: We introduce a class of collider observables, named Lund-Tree Shapes (LTS), defined from declustering trees originating from the Lund jet plane representation of the QCD radiation pattern in multi-jet scattering processes. At the differential level, they are continuous global variables akin classical event shapes and $n \rightarrow n + 1$ jet-resolution parameters, which probe the geometry and hierarchical structure of the radiation in an event. At the integrated, cumulative level, they naturally define n jet rates, providing a jet-multiplicity-based characterisation of multi-jet final states. Their definition applies to scattering processes with any number of resolved jets in the final state, as well as to groomed jets. They are thus usable as resolution variables in the context of higher-order calculations via phase-space slicing, matching fixed-order calculations to parton showers, and testing the logarithmic accuracy of shower algorithms. From a theoretical viewpoint, such observables feature a simple all-order structure and are free of non-global logarithmic corrections. As an initial application, we derive next-to-next-to-leading-logarithmic accurate predictions for processes with two QCD legs at ee , pp and ep colliders, and matched predictions to next-to-next-to-leading order for the LHC, discussing aspects of collider phenomenology.

KEYWORDS: QCD, Jets and Jet Substructure

Contents

1	Introduction	2
2	LTS definition	3
2.1	Lepton-lepton collisions	3
2.2	Hadron-hadron collisions	4
2.3	Lepton-hadron collisions	7
2.4	Groomed jets	8
3	Resummation to NNLL for the two-legs case	9
3.1	$N = 2$ case at lepton colliders	9
3.2	$N = 0$ case at hadron colliders	12
3.2.1	Results for different reference frames	16
3.2.2	Absence of non-global logarithms in the multi-jet case	19
3.2.3	Comment on possible coherence-violating effects at higher orders	21
3.3	$N = 1$ case in DIS	22
3.4	Fixed-order validation up to second perturbative order for pp	23
4	NNLL+NNLO predictions and Monte Carlo studies for the LHC	25
4.1	Matching to fixed order	25
4.2	Results at the LHC	26
4.3	Impact of multi-parton scattering and hadronisation	28
5	Conclusions	31
A	Perturbative expansion for resummation ingredients	32
A.1	Splitting functions and coefficient functions	33
A.2	The Sudakov radiator	33
A.3	The NNLL transfer function	35
A.4	Constants	39
B	A prescription for switching off logarithms in matching	41
C	Fixed-order validation up to second perturbative order for ep and ee	42

1 Introduction

Understanding the pattern of QCD radiation in high-energy collisions is a central goal of the modern collider-physics programme. Hard scattering events produce jets of collimated particles whose internal structure encodes fundamental aspects of strong interactions. Observables such as jet rates, event shapes, and jet substructure variables have long been used to probe this radiation, testing the accuracy of perturbative predictions and of parton showers. Yet, despite their success, many of these observables face inherent limitations: some are sensitive to non-global logarithms, others are largely affected by underlying event activity at hadron colliders, and some do not generalise easily to multi-leg scattering processes. To overcome these limitations, in this article we exploit the Lund-jet-plane [1, 2] representation of QCD radiation as a robust way to define new observables that are both theoretically tractable and experimentally accessible.

With this technology, we introduce Lund-Tree Shapes (LTS). For processes with two emitting legs, these observables were first introduced (at next-to-leading-logarithmic accuracy, NLL) for the purpose of testing the logarithmic accuracy of parton showers in ee [3], pp [4] and ep [5] collisions. In this article, we present a generalisation to processes with any number of resolved jets, as well as to the case of groomed jets. These observables serve a dual purpose. At the differential level, they act as continuous event-shape or jet-resolution-parameter like variables (cf., e.g., Refs. [6–8] and references therein for an overview), probing the fine-grained geometry of radiation pattern in multi-jet processes. At the integrated, cumulative level, the same observables naturally define jet rates, providing a resolution-based characterisation of multi-jet events and a natural definition of jet vetoes with improved theoretical properties.

The advantages of LTS are manifold. Their definition is general, applicable to events with any number of resolved jets and across different collider environments (ee , pp , ep). From a phenomenological viewpoint, they offer a tool to study the radiation pattern in multi-jet processes, and to characterise multi-jet events in terms of jet multiplicity when used as jet vetoes [9–17]. They can be also used to characterise the composition of underlying event as well as to study the structure of soft QCD radiation in multi-jet events. From a theoretical perspective, they possess simple all-order perturbative properties, avoiding complications such as non-global logarithms, and are ideally suited for use as resolution variables in phase-space slicing [18–24], matching fixed-order calculations to parton showers (e.g., specifically within the methods of Refs. [25–34]) and testing the logarithmic accuracy of event generators [3–5, 35–49]. As an application, we present new calculations at next-to-next-to-leading logarithmic (NNLL) order for 2-leg processes in ee , pp and ep (i.e. deep inelastic scattering, DIS) collisions, and provide matched predictions to next-to-next-to-leading order (NNLO) for the LHC. We also study their sensitivity to hadronisation and underlying event when used for collider phenomenology.

The paper is organised as follows. In Sec. 2 we define the LTS observables for ee (Sec. 2.1), pp (Sec. 2.2), ep (Sec. 2.3) collisions, and for groomed jets (Sec. 2.4). Their resummation up to NNLL accuracy is detailed in Sec. 3, where we also discuss the validation of our results. In Sec. 4 we consider the particular case of $pp \rightarrow Z$ production, match our

NNLL predictions to NNLO and inspect the impact of hadronisation and underlying events on the LTS. We conclude in Sec. 5. We also provide several additional details about the resummation, matching and fixed-order checks of our results in the appendix.

2 LTS definition

Our starting point to define the LTS is the definition of the Lund jet plane [1, 2]. We start with the case of final-state radiation, for instance produced in the decay of a colour singlet in lepton-lepton collisions, and then discuss the extension to hadron-hadron and lepton-hadron collisions.

2.1 Lepton-lepton collisions

We start our discussion by considering the 2-jet case, and then generalise the definition to an arbitrary jet multiplicity N in the final state. We consider the decay of a colour singlet of invariant mass $M_F \equiv Q$ and work in its rest frame. The LTS are defined as follows. We cluster the whole event with the Cambridge [50, 51] algorithm that uses the distance measure (between two proto-jets i,j)

$$d_{ij} = 2(1 - \cos \theta_{ij}), \quad (2.1)$$

until we are left with two exclusive jets $\{j_L, j_R\}$. For each of the two exclusive jets, we apply the following declustering procedure.

1. We start from the last clustering $\tilde{ij} \rightarrow i, j$, where i denotes the most energetic (harder) subjet, i.e. $E_i > E_j$. The splitting is characterised by a pair of Lund-plane coordinates. These can be chosen to be $(\eta^{(ij)}, k_t^{(ij)})$, defined as ¹

$$\eta^{(ij)} = -\ln \tan \frac{\theta_{ij}}{2}, \quad k_t^{(ij)} = E_j |\sin \theta_{ij}|. \quad (2.3)$$

2. Using the above definition (2.3), we calculate the quantity

$$v_b^{(ij)} = \frac{k_t^{(ij)}}{Q} e^{-b|\eta^{(ij)}|}, \quad (2.4)$$

where $b > -1$ as required for infrared safety. We note that additional Lund-tree variables, such as the azimuthal ψ angle [2, 3, 37, 38] could be also used to define additional variants of LTS.

¹An alternative pair of Lund-plane coordinates that can be considered is the transverse mass $m_t^{(ij)}$ and rapidity $y^{(ij)}$ defined as

$$m_t^{(ij)} = E_j \sqrt{1 - \beta_i^2 \beta_j^2 \cos^2 \theta_{ij}}, \quad y^{(ij)} = \frac{1}{2} \ln \frac{1 + \beta_i \beta_j \cos \theta_{ij}}{1 - \beta_i \beta_j \cos \theta_{ij}}, \quad (2.2)$$

where $\beta_k = |\vec{p}_k|/E_k$. One could also consider defining the clusterings using the WTA recombination scheme [52, 53] in defining the above coordinates, or using the d_{ij} variable of Ref. [54] as a transverse-momentum measure. For the sake of concreteness, we will use the pair defined in Eq. (2.3) in the following. All these variants can be calculated at NNLL using the methods discussed in this article.

3. We then go back to step 1 of this procedure following the harder subjet i , i.e. we only consider the set of *primary* declusterings $d_p^{(\tilde{i}j)}$ for each of the two jets $\{j_L, j_R\}$. These declusterings are defined by the set of the Lund coordinates $d_{p,L/R}^{(\tilde{i}j)} \equiv \{(\eta^{(\tilde{i}j)}, k_t^{(\tilde{i}j)})\}_{L/R}$, measured using all primary declusterings.

We then define the set of all declusterings in the event as

$$\mathcal{I}_{N=2} \equiv d_{p,L}^{(\tilde{i}j)} \cup d_{p,R}^{(\tilde{i}j)}, \quad (2.5)$$

where $N = 2$ denotes the number of resolved jets. We can now define the two LTS $M_b^{(N=2)}$ and $S_b^{(N=2)}$ as

$$M_b^{(2)} = \max_{j \in \mathcal{I}_2} v_b^j, \quad S_b^{(2)} = \sum_{j \in \mathcal{I}_2} v_b^j. \quad (2.6)$$

The extension to $N = 3$ jets can be done by first identifying the element j_k of \mathcal{I}_2 with the largest $v_b^{(\tilde{i}j)}$.² We then remove this from the initial list \mathcal{I}_2 , and instead add back all the primary declusterings $d_p^{(k)}$ of j_k , hence defining the new input list \mathcal{I}_3

$$\mathcal{I}_3 \equiv \{\mathcal{I}_2 \setminus j_k\} \cup d_p^{(k)}. \quad (2.7)$$

This procedure can be recursively extended for an arbitrary jet multiplicity N . That is, to build \mathcal{I}_N from \mathcal{I}_{N-1} , we identify the $\tilde{i}j \rightarrow i, j$ clustering in \mathcal{I}_{N-1} (with $E_i > E_j$) corresponding to the largest $v_b^{(\tilde{i}j)}$, remove it from the list, and add instead all the primary declusterings from jet j . With this procedure, we can define the N -jet generalisation of the 2-jet LTS of Eq. (2.6) as

$$M_b^{(N)} = \max_{j \in \mathcal{I}_N} v_b^j, \quad S_b^{(N)} = \sum_{j \in \mathcal{I}_N} v_b^j. \quad (2.8)$$

We stress that the collinear safety of the $M_b^{(N)}$ observable is guaranteed by the use of a clustering procedure.

In the $N = 2$ case, these observables were first introduced at NLL in Ref. [3] to test the logarithmic accuracy of parton showers in ee collisions. The $M_b^{(2)}$ observable with $b = 0$ is close in spirit (up to a wide-angle soft correction starting at NNLL) to the y_{23} resolution in the Cambridge algorithm [50], which is known up to NNLL [55, 56]. Similarly, the $S_b^{(2)}$ observables are related to thrust [57–59] ($b = 1$) and FC_x [60, 61] and angularities [61–63] ($b = 1 - x$) up to the NLL order, while they differ from these observables starting at NNLL.

2.2 Hadron-hadron collisions

We now extend the above definition to the hadron-collider case. We start by considering the process $pp \rightarrow F$, where F denotes a colour-singlet system of invariant mass Q . We initially work in the laboratory frame, and then discuss alternative reference frames in Sec. 3.2.1. We start by considering the case of $N = 0$ resolved jets in the final state [4]. That is

²One could also consider using other metrics in defining the *leading* third jet in the event, like for instance its transverse momentum with respect to a suitably chosen axis.

obtained by clustering the full event with the Cambridge/Aachen (C/A) algorithm [50] with radius R . These C/A jets define the input set for the definition of the LTS. We denote this by

$$\mathcal{I}_{N=0} \equiv \{j_1, j_2, \dots, j_m\}. \quad (2.9)$$

A natural pair of Lund coordinates for each jet, and the one we will use, corresponds to the rapidity and transverse momentum of the jet with respect to the beam, i.e. $(y^i, p_{t,i})$. Analogously to the lepton colliders case, using these coordinates, we calculate the quantity

$$v_b^{j_i} = p_{t,i} e^{-b|y^i|}. \quad (2.10)$$

We then define the LTS in $pp \rightarrow F$ with $N = 0$ as

$$M_b^{(0)} = \max_{j \in \mathcal{I}_0} v_b^j, \quad S_b^{(0)} = \sum_{j \in \mathcal{I}_0} v_b^j. \quad (2.11)$$

This procedure can be extended to the $N = 1$ case (e.g. measured in $pp \rightarrow F + \text{jet}$) by removing from the input list \mathcal{I}_0 the jet with the largest $v_b^{j_i}$, that we denote by j_k . We then add the list of primary declusterings $d_p^{(k)}$ of j_k , namely

$$\mathcal{I}_1 \equiv \{\mathcal{I}_0 \setminus j_k\} \cup d_p^{(k)}. \quad (2.12)$$

The list of declusterings $d_p^{(k)}$ of the removed jet j_k from \mathcal{I}_0 is constructed as follows.

1. Starting from the last C/A clustering step $\tilde{ij} \rightarrow i, j$ in j_k , we denote with i the most energetic subjet, i.e. $p_{t,i} > p_{t,j}$. We associate to this splitting a pair of Lund-plane coordinates $(y^{(\tilde{ij})}, k_t^{(\tilde{ij})})$ on the Lund-plane leaf created by the jet j_k . These are a measure of the transverse momentum and rapidity of the softer subjet j with respect to the harder subjet i . They can be defined as ³

$$y^{(\tilde{ij})} = |y^k| - \ln \frac{\Delta R_{ij}}{R}, \quad k_t^{(\tilde{ij})} = p_{t,j} \frac{\Delta R_{ij}}{R}, \quad \Delta R_{ij} \equiv \sqrt{\Delta y_{ij}^2 + \Delta \phi_{ij}^2}, \quad (2.13)$$

where y_k is the rapidity of the jet j_k . The $|y^k|$ term ensures that the rapidity of a clustering close to the jet boundary approaches that of the jet itself. This aspect is ultimately important to guarantee the absence of non-global logarithms in the LTS (see Section 3.2.2). Note that $|y^{(\tilde{ij})}| \gg 1$ when the two subjets are collinear.

2. On this splitting we calculate

$$v_b^{(\tilde{ij})} = k_t^{(\tilde{ij})} e^{-b|y^{(\tilde{ij})}|}. \quad (2.14)$$

3. Go back to step 1 of this procedure following the harder subjet i .

The resulting list of primary declusterings defines $d_p^{(k)}$. Two example configurations are illustrated in Fig. 1.

³An alternative definition involves the rapidity of i w.r.t. j given by $y^{(\tilde{ij})} = \frac{1}{2} \ln \frac{E_j + \vec{p}_j \cdot \hat{n}_i}{E_j - \vec{p}_j \cdot \hat{n}_i}$ where $\hat{n}_i \equiv \vec{p}_i / |\vec{p}_i|$. One could also define the Lund transverse momentum as $k_t^{(\tilde{ij})} = p_{t,j} \Delta R_{ij}$, as done in the original Lund-jet-plane paper [2].

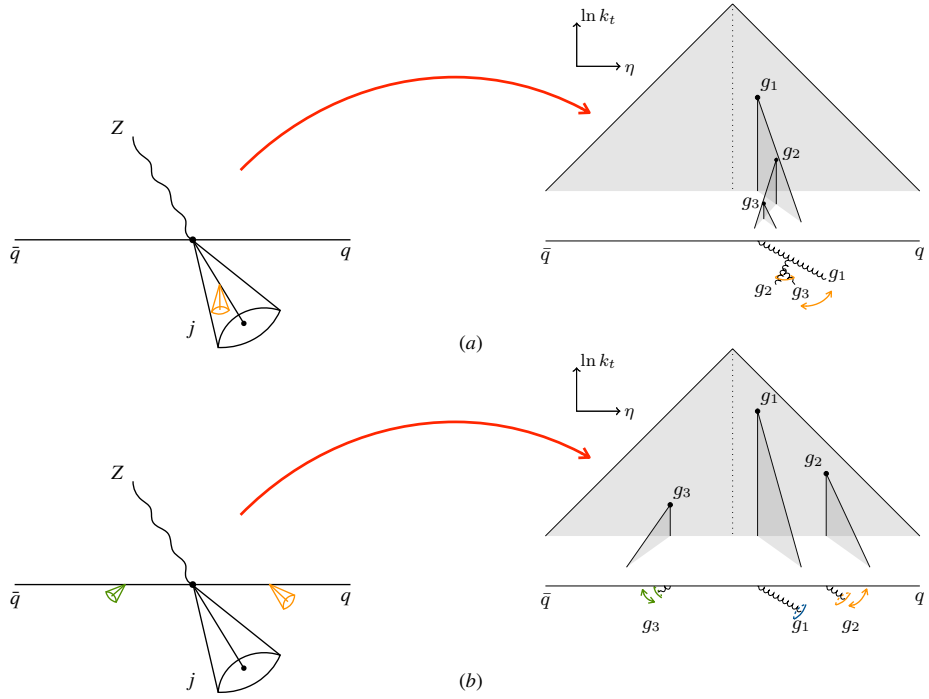


Figure 1: An illustration of LTS for two Z +jet events: (a) In this event there are no primary declusterings from the beam, while the jet contains a primary declustering resulting from the recombination of emissions g_2 and g_3 ; (b) In this event the jet contains no primary declusterings, while there are two primary declusterings from the beam corresponding to the (primary) emissions g_2 and g_3 . The two-sided arrows indicate the Lund measures that enter the definition of the LTS.

This procedure can be iterated to the case with N jets. For instance, for $N = 2$, the input list \mathcal{I}_2 is obtained by removing the element of \mathcal{I}_1 with the largest v_b (either one of the $v_b^{(ij)}$ or one of the v_b^{ji}) and adding its list of primary declusterings. The general LTS are then defined by

$$M_b^{(N)} = \max_{j \in \mathcal{I}_N} v_b^j, \quad S_b^{(N)} = \sum_{j \in \mathcal{I}_N} v_b^j. \quad (2.15)$$

So far, we have defined the LTS in the laboratory frame. In some cases it can be interesting to consider the definition in a different reference frame. An example is the process $pp \rightarrow F$ ($N = 0$), where one may want to work in a frame where the colour singlet F has zero rapidity, $y_F = 0$, that is the partonic centre-of-mass (c.o.m.) frame. The corresponding definition of the LTS (2.11) is then expressed in terms of the quantity

$$v_b^{ji} = p_{t,i} e^{-b|y^i - y_F|}. \quad (2.16)$$

This will affect the resummation at NNLL. We will come back to this in Sec. 3.2.1.

In the $N = 0$ case, these observables were first introduced at NLL in Ref. [4] to test the logarithmic accuracy of parton showers in pp collisions. For $N = 0$, observables of the kind written in Eq. (2.15) have been considered before in the literature. Observables related to $M_b^{(0)}$ have been previously studied in the context of jet vetoes in Refs. [9–13] ($b = 0$) and

Refs. [14, 16, 17] ($b = 1$). These types of jet vetoes agree with $M_b^{(0)}$ for $b = 0$ up to NNLL, but they differ beyond this order due to the details of the jet algorithm (anti- k_t v. C/A) as well as at fixed order starting from NNLO by subleading-power corrections. Instead, for $b = 1$, they differ starting at NNLL from the rapidity-dependent jet vetoes computed and studied in Refs. [16, 17], due to their use of the transverse mass instead of transverse momentum in the observable definition. The latter would correspond to a different variant of LTS, not considered here. At pp colliders, the LTS constitute a *global* generalisation of jet vetoes to the multi-jet case. The $S_b^{(0)}$ observables are also related to beam thrust [64] ($b = 1$) and E_T [65–69] ($b = 0$) up to NLL, but they differ from these at higher orders.

We note that, in contrast with the e^+e^- case where the total energy is known, in pp we defined the LTS to have mass dimension one. While in the $pp \rightarrow F$ case one could normalise the transverse momentum by Q , one has some freedom in defining the hard scale in the N -jet case, where multiple scales in the scattering process are present. For the sake of simplicity, in the $N = 0$ resummed calculations given in Sec. 3 we will normalise $M_b^{(0)}$ and $S_b^{(0)}$ by Q so that they are dimensionless. That is, for the rest of this article, we define the dimensionless counterpart of the observables in the pp case as

$$v_b^{j_i} = \frac{p_{t,i}}{Q} e^{-b|y^i|}, \quad M_b^{(0)} = \max_{j \in \mathcal{I}_0} v_b^j, \quad S_b^{(0)} = \sum_{j \in \mathcal{I}_0} v_b^j, \quad (2.17)$$

with Q being the invariant mass of the colour singlet. An analogous definition holds for the partonic c.o.m. frame variant.

2.3 Lepton-hadron collisions

For DIS, it is convenient to start by considering a single final-state jet and then generalise the definition to arbitrary jet multiplicities.

We work in the Breit frame [70], defined such that the incoming parton has energy exactly equal to the total energy of the final-state partons, and the momentum transfer

$$q_{\text{dis}}^\mu = q_{\text{out}}^\mu - q_{\text{in}}^\mu \quad (2.18)$$

is space-like. In this frame, the incoming parton is conventionally chosen to be anti-aligned with the z axis.

The event is then clustered using the Cambridge algorithm, in analogy with the lepton-collider case (see Sec. 2.1). Alongside the usual pairwise distance

$$d_{ij} = 2(1 - \cos \theta_{ij}) \quad (2.19)$$

between proto-jets, we also consider the distance to the beam,

$$d_{iB} = 2(1 - \cos \theta_{iB}), \quad (2.20)$$

and proceed with clustering the event into jets in the standard manner.

All resulting jets correspond to primary emissions from the initial state, except for the one originating from the fragmentation of the original final-state parton, which we

denote as j_k . This jet is identified as the one carrying the largest light-cone component anti-parallel to the incoming parton in the Breit frame. Operationally, it is the jet whose momentum maximises the scalar product with the proton momentum.

We then decluster this final-state jet following the same procedure as in the lepton-collider case, denoting the list of its primary declusterings by $d_p^{(k)}$. If \mathcal{I}_0 denotes the list of primary declusterings from initial-state radiation, the complete list of primary declusterings for DIS is

$$\mathcal{I}_1 = \{\mathcal{I}_0 \setminus j_k\} \cup d_p^{(k)}. \quad (2.21)$$

As in the lepton- and hadron-collider cases, there is some freedom in defining the Lund coordinates that enter the definition of the LTS. In the following, we adopt the coordinates in Eq. (2.3), replacing the angle θ_{ij} with θ_{iB} for initial-state declusterings.

The LTS are then defined as in Eq. (2.4) with

$$Q = \sqrt{-q_{\text{dis}}^2}. \quad (2.22)$$

The $N = 2$ definition is obtained from the $N = 1$ case by replacing, in \mathcal{I}_1 , the declustering with the largest v_b (either an initial- or final-state declustering) with its own primary declusterings. Higher jet multiplicities are obtained recursively following the same procedure.

In the $N = 1$ case, these observables were first introduced at NLL in Ref. [5] to test the logarithmic accuracy of parton showers in ep collisions. For $N = 1$, observables of the $S_b^{(1)}$ type with $b = 1$ are similar to 1-jettiness or one of the variants of DIS thrust [71–75] up to NLL, but not beyond.

2.4 Groomed jets

The LTS variables also serve as jet substructure observables when, for instance, measured on jets groomed with the Soft-Drop [76] or mMDT [77] grooming procedure. Their definition now applies to the Lund declusterings within an energetic jet that passes the grooming condition. This variant of the LTS features a milder sensitivity to hadronisation and underlying event at hadron colliders, enabling the study of the structure of QCD jets. To define them, we consider a jet J (this can be, for instance, an anti- k_t jet at pp colliders or a hemisphere defined with respect to the thrust/WTA axis at ee colliders), and groom its content with the Soft-Drop/mMDT grooming procedure, with grooming parameter z_{cut} (and β in the Soft-Drop case). We now apply the Lund-jet declustering [2] to the resulting groomed jet and denote the list of its *primary* Lund declusterings by

$$\mathcal{I}_{J_{\text{SD}}} \equiv d_{p, \text{SD}}^{(J)}, \quad (2.23)$$

constructed as outlined in the previous sections depending on the type of collider environment considered. Each declustering is characterised by the usual set of Lund-plane coordinates $(k_t^{(ij)}, y^{(ij)})$. For each of these declusterings we calculate $v_{b, \text{SD}}^{(ij)} = k_t^{(ij)} e^{-b|y^{(ij)}|}$. The groomed LTS (gLTS) are then defined by

$$M_{b, \text{SD}} = \max_{j \in \mathcal{I}_{J_{\text{SD}}}} v_{b, \text{SD}}^j, \quad S_{b, \text{SD}} = \sum_{j \in \mathcal{I}_{J_{\text{SD}}}} v_{b, \text{SD}}^j. \quad (2.24)$$

They can be normalised to hard scale of the jet, i.e. its pre-grooming transverse momentum (pp colliders) or energy (ee colliders). The resummation structure of these observables for $\beta = 0$, in the limit $v \ll z_{\text{cut}}$, can be studied, for instance, with the methods of Refs. [78–86]. For $\beta > 0$ additional complications related to non-global logarithms may arise. An alternative definition of the groomed LTS would directly use the Soft-Drop/mMDT grooming procedure at the level of the declusterings that enter the LTS, that is similar in spirit to using a recursive soft-drop procedure [87]. We do not pursue the groomed versions further here, and leave their detailed study to future work.

3 Resummation to NNLL for the two-legs case

In this section we discuss the resummation properties of the LTS, and perform explicit calculations up to the NNLL order in the case of processes with 2 radiating legs at the lowest order. We will start with a discussion of the lepton-collider case, and then illustrate the hadron-collider and DIS cases.

3.1 $N = 2$ case at lepton colliders

The LTS at lepton colliders have a very simple resummation structure. We adopt the resummation formalism of Refs. [55, 56, 61, 88], in which one expresses the (non-normalised) cumulative cross section for a given observable $v \in \{M_b^{(2)}, S_b^{(2)}\}$ as follows

$$\Sigma^{ee}(v) \equiv \int_0^v dv' \frac{d\sigma}{dv'} = \Sigma_S^{ee}(v) \mathcal{F}^{ee}(v). \quad (3.1)$$

The explicit expressions of the ingredients of the above equation depend on whether we are considering a Born final state consisting of two quark jets (Z decay) or two gluon jets (H decay). To keep the notation light, we suppress the dependence on the flavour of the final state in this section. However we provide results for both quark and gluon jets in Appendix A.

The factor $\Sigma_S^{ee}(v)$ denotes the cumulative distribution for a simplified version of the observable. Its definition proceeds by classifying the multi-parton squared matrix elements into correlated clusters of emissions [61], namely the building blocks of the multi-parton squared amplitudes that vanish in the limit where emissions are widely separated in rapidity. In practice, this classification can be implemented recursively. For concreteness, let us consider the soft limit. In this regime, matrix elements factorise into independent eikonal factors whenever emissions, or subsets of emissions, are widely separated in rapidity. With two emissions, one can thus identify an uncorrelated contribution obtained in the limit where the two emissions are widely separated. The correlated contribution is then defined as the remainder, which by construction only has support in the region where the two emissions have comparable rapidities. This recursive definition extends naturally to higher multiplicities [61].⁴ An analogous organisation can be carried out in the collinear limit.

⁴For example, for three emissions, the procedure generalises as follows. One first subtracts the fully uncorrelated contribution, corresponding to three widely separated emissions, which factorises into a product of three independent eikonal factors. Next, one removes the three configurations in which a pair of

One then calculates the quantity

$$v_b(k) = \frac{k_t}{Q} e^{-b|y|}, \quad (3.2)$$

for each of the correlated clusters, and defines the simplified observable to be the largest of these.

This definition leads to a remarkably simple resummation structure that, at NNLL order, can be cast as

$$\Sigma_S^{ee}(v) = \sigma^{(0)} \left(1 + \frac{\alpha_s(\mu_R)}{2\pi} H^{(1)} + \sum_{\ell=1}^2 \frac{\alpha_s(\mu_R)}{2\pi} \frac{1+b}{1+b-2\lambda} C_{\text{hc},\ell}^{(1)} \right) \exp\{-\mathcal{R}_{\text{NNLL}}(v)\}, \quad (3.3)$$

where $\sigma^{(0)}$ is the Born cross-section and $\lambda = \alpha_s(\mu_R)\beta_0 L$, with L being the large logarithms to resum (cf. Eq. (A.1)). The constant $H^{(1)}$ ($C_{\text{hc}}^{(1)}$) stems from the hard (hard-collinear) region. The sums over ℓ reflect the presence of two legs in the process. All constants as a function of the parameter b are given in Appendix A.4. The NNLL Sudakov radiator $\mathcal{R}_{\text{NNLL}}(v)$, which is a function of the parameter b , can be written as a sum of contributions $R_\ell(v)$ from each emitting leg ℓ , which can be in turn decomposed into a soft and collinear term

$$\mathcal{R}_{\text{NNLL}}(v) = \sum_{\ell=1}^2 R_\ell(v) = \sum_{\ell=1}^2 \left[R_s^\ell(v) + R_{\text{hc}}^\ell(v) \right]. \quad (3.4)$$

At NNLL accuracy, the soft radiator R_s^ℓ reads

$$R_s^\ell(v) = -\frac{\lambda}{\alpha_s \beta_0} g_1^\ell(\lambda) - g_2^\ell(\lambda) - \frac{\alpha_s}{\pi} \left(g_3^\ell(\lambda) + \delta g_3^\ell(\lambda) \right), \quad (3.5)$$

and the hard-collinear radiator reads

$$R_{\text{hc}}^\ell(v) = -h_2^\ell(\lambda) - \frac{\alpha_s}{\pi} h_3^\ell(\lambda). \quad (3.6)$$

The functions g_i^ℓ , δg_3^ℓ and h_i^ℓ are provided in Appendix A. An important aspect of the definition of the simplified observable is that it agrees with the full observable at LL.

Let us now consider the second factor in the r.h.s. of Eq. (3.1), the *transfer function* $\mathcal{F}^{ee}(v)$. As the name suggests, this accounts for the difference between the full observable that is being resummed, in this case either $M_b^{(2)}$ or $S_b^{(2)}$, and the simplified observable encoded in Σ_S^{ee} . By definition, it is given by

$$\mathcal{F}^{ee}(v) \equiv \frac{\Sigma^{ee}(v)}{\Sigma_S^{ee}(v)}. \quad (3.7)$$

This object has the following key properties. Firstly, since by definition $\Sigma_S(v)$ contains all the LL corrections, the transfer function starts at NLL order. Secondly, the transfer function is finite in $D = 4$ space-time dimensions, which crucially makes it amenable to

emissions is widely separated from the third, which factorise into a single emission and a correlated pair. The remaining term then represents the contribution from three correlated emissions.

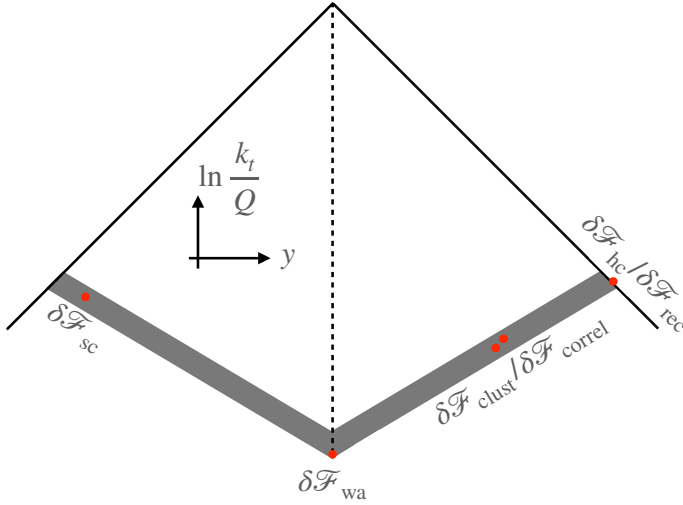


Figure 2: Location of NNLL corrections to the transfer function in the Lund plane of the Born $q\bar{q}$ system.

a numerical computation. To make this fact manifest, it is customary to introduce a resolution parameter δ and recast Eq. (3.7) as

$$\mathcal{F}^{ee}(v) = \lim_{\delta \rightarrow 0} \frac{\Sigma^{ee}(v)}{\Sigma_S^{ee}(\delta v)} \frac{\Sigma_S^{ee}(\delta v)}{\Sigma_S^{ee}(v)}, \quad (3.8)$$

which can be directly used for practical calculations. The fact that Eq. (3.8) is finite in the limit $\delta \rightarrow 0$ stems from the recursive IRC (rIRC) safety [60] of LTS: emissions that contribute to $\Sigma^{ee}(v)$ with a $v_b \leq \delta v$ can be neglected in the evaluation of the observable. Therefore, their contribution to $\Sigma^{ee}(v)$ factorises from the one of resolved emissions (i.e. with $v_b > \delta v$) and cancels against the denominator $\Sigma_S^{ee}(\delta v)$. The residual dependence on δ will now balance that of the ratio $\Sigma_S^{ee}(\delta v)/\Sigma_S(v)$, leading to a result that is finite in the $\delta \rightarrow 0$ limit. Following Refs. [56, 61, 88, 89], at NNLL these corrections can be parameterised as follows

$$\mathcal{F}^{ee}(v) = \mathcal{F}_{\text{NLL}}^{ee}(v) + \frac{\alpha_s(\mu_R)}{\pi} \delta \mathcal{F}_{\text{NNLL}}^{ee}(v), \quad (3.9a)$$

$$\delta \mathcal{F}_{\text{NNLL}}^{ee}(v) = \delta \mathcal{F}_{\text{sc}}^{ee}(v) + \delta \mathcal{F}_{\text{wa}}^{ee}(v) + \delta \mathcal{F}_{\text{rec}}^{ee}(v) + \delta \mathcal{F}_{\text{hc}}^{ee}(v) + \delta \mathcal{F}_{\text{correl}}^{ee}(v) + \delta \mathcal{F}_{\text{clust}}^{ee}(v). \quad (3.9b)$$

The structure of Eq. (3.9) can be understood with a simple power counting argument, that can be explained with the help of the primary Lund plane in Fig. 2.

At NLL order, $\mathcal{F}_{\text{NLL}}^{ee}(v)$ is described by an ensemble of multiple soft *and* collinear emissions widely separated in rapidity, each having a value v_i of the observable, with $\delta v \leq v_i \leq v$. This is represented by the shaded region adjacent to the observable boundary in Fig. 2, which is populated by such emissions.

Beyond NLL, $\mathcal{F}^{ee}(v)$ must encode corrections in regions of the Lund plane that are parameterically suppressed by $\mathcal{O}(\alpha_s)$ (counting $L \sim 1/\alpha_s$) with respect to the NLL limit. Each of the terms in Eq. (3.9) encodes one of these corrections in different kinematic limits (cf. discussion in Refs. [56, 61, 88] for more details). In short, these are:

- An extra pair of soft-collinear emissions becoming close in rapidity. This correction is encoded into the $\delta\mathcal{F}_{\text{correl}}^{ee}(v)$ (involving the correlated part of the double-soft squared amplitude) and $\delta\mathcal{F}_{\text{clust}}^{ee}(v)$ (involving the uncorrelated, independent part of the double-soft squared amplitude). This contribution starts with terms of order $\alpha_s^2 L$.
- A single extra soft emission at wide angle w.r.t. the event direction, encoded in the correction $\delta\mathcal{F}_{\text{wa}}^{ee}(v)$. This correction encodes the difference between the observable and the simple observable for a soft gluon radiated with a wide angle w.r.t. its emitter. This contribution starts at order α_s .
- A single extra hard-collinear emission, giving rise to the corrections $\delta\mathcal{F}_{\text{rec}}^{ee}(v)$ and $\delta\mathcal{F}_{\text{hc}}^{ee}(v)$. The former, $\delta\mathcal{F}_{\text{rec}}^{ee}(v)$ is the recoil correction which encodes the difference between the observable and the simple observable in the presence of a hard-collinear splitting kinematics. The latter, $\delta\mathcal{F}_{\text{hc}}^{ee}(v)$, accounts for the correction to the matrix element.
- A single extra soft-collinear emission, with a higher-order kernel containing running-coupling terms in the CMW scheme [61, 90, 91] as well as with the correct rapidity bound which was approximated at NLL.⁵ This correction defines $\delta\mathcal{F}_{\text{sc}}^{ee}(v)$.

All the ingredients are provided in Appendix A. In our numerical implementation, we expand out the product $\Sigma_S \mathcal{F}_{\text{NNLL}}$ in Eq. (3.1) so that $\delta\mathcal{F}_{\text{NNLL}}$ multiplies only the exponential of the Sudakov radiator $\exp\{-\mathcal{R}_{\text{NNLL}}(v)\}$, i.e. without the $\mathcal{O}(\alpha_s)$ constant pre-factor in Eq. (3.3). This throws away subleading N^3LL terms.

3.2 $N = 0$ case at hadron colliders

We will first consider the observable defined in the partonic c.o.m. frame (cf. Eq. (2.16) and discussion thereof) where the colour singlet has zero rapidity. We will then discuss the laboratory-frame definition of the LTS in Sec. 3.2.1. In the hadron-collider case, the structure of the NNLL resummation for the cumulative distribution $\Sigma^{pp}(v)$ has to be modified with respect to the lepton-collider form given in Eq. (3.1). A first difference with the lepton-collider case is due to the precise definition of the observable, and specifically to the different jet algorithm and the definitions of transverse momentum and rapidity adopted, as discussed in Sec. 2.2. This will modify the correlated and clustering corrections, whose expressions are reported in Appendix A. A second key difference is due to the presence of initial-state radiation (ISR) that modifies the structure of the resummation of collinear logarithms, both in the simple observable $\Sigma_S(v)$, as well as in the form of the transfer function \mathcal{F} .

To gain intuition, it is instructive to consider the NNLL transfer function defined in Eq. (3.9) in the final-state radiation (FSR) case. Among the six NNLL corrections to \mathcal{F}^{ee} ,

⁵At NLL one expands the rapidity bound for each emission about the hard collinear scale, namely $|\eta| \leq \ln \frac{Q}{k_t} \simeq \frac{1}{1+b} \ln \frac{1}{v}$.

four originate from soft dynamics. In the initial-state radiation (ISR) case, these soft corrections do not modify the longitudinal momentum fractions of the incoming partons, and hence their functional form remains identical to that of the FSR case (up to modifications arising from the differences between observables, as discussed above).

In contrast, the hard-collinear and recoil corrections account for the effects of hard-collinear splittings in the final state. The hard-collinear correction describes the modification of the matrix element due to the emission of hard-collinear radiation, while treating the corresponding kinematics as soft. The recoil correction, on the other hand, captures the impact of the recoil induced by the hard-collinear emission on the observable.

In the ISR case, the corrections associated with an initial-state hard-collinear splitting differ in several respects. First, since the beam direction, and hence the observable, is unaffected by transverse recoil, the corresponding recoil correction is absent. Second, the hard-collinear correction remains unchanged, as it reflects a modification of the matrix element rather than of the emission kinematics, which are treated as soft. Consequently, this correction does not alter the longitudinal momentum fractions of the incoming partons. In addition, a new correction arises, accounting for the longitudinal recoil induced by the hard-collinear emission. We refer to this as the DGLAP correction, which will be discussed in detail below. This correction replaces the recoil correction present in the FSR case.

To derive the NNLL resummation formula, we start by defining the contribution of the simple observable, $\Sigma_S^{pp}(v)$. The *simple* observable in the hadron-collider case can be defined analogously to its lepton-collider counterpart given in Eq. (3.2), where now the transverse momentum k_t and rapidity y are taken in the c.o.m. frame of the partonic scattering. To formalise the discussion, we consider the production of a colour singlet system F in a pp collision. For simplicity we assume this production process to be mediated by a single flavour channel (either quark or gluon initiated). At the parton level, we will denote the flavour of the two partons initiating the Born process by c, d . For processes that receive a contribution from different flavour channels one should repeat the discussion below for each of the relevant channels and add them together. With a slight abuse of notation, we denote the cumulative cross section differential in the kinematics of the final state at the Born level by $\Sigma(v, \Phi_B) \equiv d\Sigma/d\Phi_B$. The resummation for the simple observable at NNLL takes the form

$$\begin{aligned} \Sigma_S^{pp}(v, \Phi_B) = & \frac{d\hat{\sigma}_{cd}^{(0)}}{d\Phi_B} \exp\{-\mathcal{R}_{\text{NNLL}}(v)\} \left[f_c(x_c, \mu_{\text{ISR}}) f_d(x_d, \mu_{\text{ISR}}) \left(1 + \frac{\alpha_s(\mu_R)}{2\pi} H_{cd}^{(1)}(\Phi_B) \right) \right. \\ & \left. + \frac{\alpha_s(\mu_R)}{2\pi} \frac{1+b}{1+b-2\lambda} \sum_i \left((C_{ci}^{(1)} \otimes f_i)(x_c, \mu_{\text{ISR}}) f_d(x_d, \mu_{\text{ISR}}) + \{c \leftrightarrow d\} \right) \right], \end{aligned} \quad (3.10)$$

where $\hat{\sigma}_{cd}^{(0)}$ is the Born partonic cross section for the cd flavour channel and $C_{ci}^{(1)}$ are one-loop, b -dependent coefficient functions (see Appendix A). The longitudinal momentum fractions $x_{c,d}$ are defined as

$$x_{c,d} = \frac{Q}{\sqrt{s}} e^{\pm y_F}, \quad (3.11)$$

and Q and y_F denote the invariant mass and the rapidity of the colour singlet F produced in the hadronic collision of c.o.m. energy \sqrt{s} . The ISR scale μ_{ISR} is defined as

$$\mu_{\text{ISR}} = \mu_F e^{-\frac{L}{1+b}}. \quad (3.12)$$

The expressions of all the ingredients in Eq. (3.10) are given in Appendix A. In Eq. (3.10), the Sudakov radiator $\mathcal{R}_{\text{NNLL}}(v)$ depends on the flavour configuration of the initial-state partons c and d , but it is flavour diagonal. Here we suppress the dependence on the flavour indices to simplify the notation. Conversely, the coefficient functions $C_{ij}^{(1)}$ modify the flavour of the initial partons flowing into the hard scattering. The operator \otimes denotes the standard convolution over the longitudinal momentum fraction given by

$$(f \otimes g)(x) = \int_x^1 \frac{dz}{z} f(z) g\left(\frac{x}{z}\right). \quad (3.13)$$

We now discuss the transfer function. Starting at NNLL, the emission of hard-collinear radiation modifies the longitudinal momentum fraction of the initial-state partons. Therefore, the cumulative cross section $\Sigma^{pp}(v, \Phi_B)$ cannot be expressed as a simple product of $\Sigma_S^{pp}(v, \Phi_B)$ and a transfer function in momentum space. Instead, this factorised, multiplicative structure holds after taking a double Mellin transform over the momentum fractions x_c and x_d (see, for instance, the discussion in Ref. [92]). When expressed in momentum space, up to NNLL accuracy, the cumulative distribution $\Sigma^{pp}(v, \Phi_B)$ can be conveniently cast as

$$\Sigma^{pp}(v, \Phi_B) = \Sigma_S^{pp}(v, \Phi_B) \mathcal{F}^{pp}(v) + \delta \Sigma_{\text{DGLAP}}^{pp}(v, \Phi_B), \quad (3.14)$$

where

$$\mathcal{F}^{pp}(v) = \mathcal{F}_{\text{NLL}}^{pp}(v) + \frac{\alpha_s(\mu_R)}{\pi} \delta \mathcal{F}_{\text{NNLL}}^{pp}(v), \quad (3.15a)$$

$$\delta \mathcal{F}_{\text{NNLL}}^{pp}(v) = \delta \mathcal{F}_{\text{sc}}^{pp}(v) + \delta \mathcal{F}_{\text{wa}}^{pp}(v) + \delta \mathcal{F}_{\text{hc}}^{pp}(v) + \delta \mathcal{F}_{\text{correl}}^{pp}(v) + \delta \mathcal{F}_{\text{clust}}^{pp}(v). \quad (3.15b)$$

Above we have omitted the simple dependence of \mathcal{F}^{pp} on the invariant mass Q of the singlet system and on the flavour of the initial-state partons. As anticipated, in Eqs. (3.15b) the recoil correction is absent, and the new DGLAP correction is included in Eq. (3.14). In the above decomposition, the NNLL transfer function $\mathcal{F}^{pp}(v)$ encodes the effect of emissions that do not affect the longitudinal momentum fraction of the initial-state partons. These are either terms of soft origin, that correspond to the hadron-collider counterpart of the terms $\mathcal{F}_{\text{NLL}}^{ee}$, $\delta \mathcal{F}_{\text{sc}}^{ee}$, $\delta \mathcal{F}_{\text{wa}}^{ee}$, $\delta \mathcal{F}_{\text{correl}}^{ee}$, $\delta \mathcal{F}_{\text{clust}}^{ee}$ in Eq. (3.9), or corrections to the squared amplitude in the hard-collinear limit, corresponding to $\delta \mathcal{F}_{\text{hc}}^{ee}$. Their calculation can be carried out exactly as in the lepton-collider case, with the only difference being in the functional form of the observable which is different in the hadron-collider case. Their expressions are reported in Appendix A.

The new term $\delta \Sigma_{\text{DGLAP}}^{pp}$ describes the change in the longitudinal momentum fraction (i.e. longitudinal recoil) of the initial-state partons. To understand the structure of $\delta \Sigma_{\text{DGLAP}}^{pp}$, it is instructive to study the contribution of an initial-state, hard-collinear emission to the cross section. To be concrete, let us consider the case of a quark initiated

process (e.g. Drell-Yan) and consider the flavour-diagonal $q \rightarrow q$ transition mediated by the emission of initial-state gluons. The corresponding contribution of one hard-collinear emission to the real radiation is obtained by integrating, over the emission phase space, the emission probability

$$\frac{\alpha_s(k_t)}{2\pi} \frac{d\phi}{2\pi} \frac{dk_t}{k_t} \frac{dz}{z} P_{qq}^{(0)}(z) f_c\left(\frac{x_c}{z}, \mu\right) f_d(x_d, \mu) + \{c \leftrightarrow d\}, \quad (3.16)$$

where $P_{qq}^{(0)}(z)$ denotes the tree-level unregularised splitting functions, cf. Appendix A. It is convenient to recast Eq. (3.16) into the sum of a term that encodes the change in the longitudinal momentum fraction of the incoming parton and a term that does not modify it. This can be done by recasting Eq. (3.16) as

$$\begin{aligned} \frac{d\phi}{2\pi} \frac{dk_t}{k_t} dz \frac{\alpha_s(k_t)}{2\pi} & \left[\left(\frac{2C_F}{1-z} + \gamma_q \delta(1-z) \right) f_c(x_c, \mu) f_d(x_d, \mu) \right. \\ & \left. + \frac{\hat{P}_{qq}^{(0)}(z)}{z} f_c\left(\frac{x_c}{z}, \mu\right) f_d(x_d, \mu) + \{c \leftrightarrow d\} \right], \end{aligned} \quad (3.17)$$

with \hat{P} now denoting the regularised splitting function and $\gamma_q = -3/2 C_F$. The parameterisation in Eq. (3.17) conveniently singles out the terms in the real radiation that modify the longitudinal momentum fraction of the incoming partons (second term in Eq. (3.17)), which will be encoded in the new contribution to the transfer function $\delta\Sigma_{\text{DGLAP}}^{pp}$. Instead, the first term in Eq. (3.17) will be accounted for in various parts of $\mathcal{F}^{pp}(v)$ in Eq. (3.15), namely \mathcal{F}_{NLL} , $\delta\mathcal{F}_{\text{sc}}^{pp}(v)$ and $\delta\mathcal{F}_{\text{hc}}^{pp}(v)$ (cf. Refs. [56, 60, 88]).

The derivation of $\delta\Sigma_{\text{DGLAP}}^{pp}$ can be easily performed in Mellin space, where the transform of the cumulative cross section $\Sigma^{pp}(v, \Phi_B)$ can be expressed as a *product* of the transform of $\Sigma_S^{pp}(v, \Phi_B)$ and a transfer function.⁶ In this space, the Mellin transform of $\delta\Sigma_{\text{DGLAP}}^{pp}$ arises from considering a single insertion (at NNLL) of the Mellin-transform of the second term in Eq. (3.17) in an ensemble of initial-state, soft-collinear emissions widely separated in rapidity. Its inverse transform yields the momentum space expression can be written as

$$\begin{aligned} \delta\Sigma_{\text{DGLAP}}^{pp}(v, \Phi_B) = \lim_{\delta \rightarrow 0} \frac{d\hat{\sigma}_{cd}^{(0)}}{d\Phi_B} e^{-\mathcal{R}_{\text{NLL}}(\delta v)} & \left\{ \sum_{n=0}^{\infty} \frac{1}{n!} \prod_{i=1}^n \int_{\delta}^1 \frac{d\zeta_i}{\zeta_i} \mathcal{R}'_{\text{NLL}}(v) \right. \\ & \times \frac{\alpha_s(Qv^{\frac{1}{1+b}})}{\pi(1+b)} \int_{\delta}^1 \frac{d\zeta_{\text{hc}}}{\zeta_{\text{hc}}} \left(\int_{x_c}^1 \frac{dz}{z} \hat{P}_{qq}^{(0)}(z) f_c\left(\frac{x_c}{z}, Qv^{\frac{1}{1+b}}\right) f_d\left(x_d, Qv^{\frac{1}{1+b}}\right) + \{c \leftrightarrow d\} \right) \\ & \left. \times [\Theta(v - V(\{\zeta_i\}, \zeta_{\text{hc}})) - \Theta(1 - \zeta_{\text{hc}})\Theta(v - V(\{\zeta_i\}))] \right\}, \end{aligned} \quad (3.18)$$

where we define $\zeta_i = v_i/v$ and $V(\{\zeta_i\})$ ($V(\{\zeta_i\}, \zeta_{\text{hc}})$) denotes the the observable in the presence of an ensemble of soft-collinear emissions $\{\zeta_i\}$ (and one hard-collinear emission ζ_{hc}) all widely separated in rapidity in the partonic c.o.m. frame. The structure of Eq. (3.18) can be understood as follows. The $\mathcal{R}'_{\text{NLL}}(v)$ kernels (cf. Appendix A) describe the emission of

⁶This product is to be understood as a matrix product in flavour space.

widely-separated, soft-collinear radiation from the initial state legs. The regularised kernel \hat{P} describes instead the insertion of a single hard-collinear emission, also widely separated in rapidity from the rest of the radiation. For the latter, the scale of the coupling and that of the parton densities is expanded, with NNLL accuracy, about the value of the transverse momentum of the hard-collinear emission that is set by the observable, that is $v = v_b(k_{\text{hc}}) = (k_{t,\text{hc}}/Q)^{1+b}$, which leads to $k_{t,\text{hc}} = Qv^{\frac{1}{1+b}}$.

The generalisation to any flavour channel, including the non-diagonal ones, simply amounts to the following replacement

$$\hat{P}_{q\bar{q}}^{(0)}(z)f_c\left(\frac{x_c}{z}, Qv^{\frac{1}{1+b}}\right) \rightarrow \sum_i \hat{P}_{ci}^{(0)}(z)f_i\left(\frac{x_c}{z}, Qv^{\frac{1}{1+b}}\right), \quad (3.19)$$

and similarly for $c \leftrightarrow d$. For the two observables considered in this article, we have

$$V(\{\zeta_i\}, \zeta_{\text{hc}}) = \sum_i \zeta_i + \zeta_{\text{hc}}, \quad \text{for } S_b^{(0)}, \quad (3.20)$$

$$V(\{\zeta_i\}, \zeta_{\text{hc}}) = \max\{\{\zeta_i\}, \zeta_{\text{hc}}\}, \quad \text{for } M_b^{(0)}, \quad (3.21)$$

leading to $\delta\Sigma_{\text{DGLAP}}^{pp}(v) = 0$ for $M_b^{(0)}$, while for $S_b^{(0)}$ one finds

$$\begin{aligned} \delta\Sigma_{\text{DGLAP}}^{pp}(v) &= \frac{d\hat{\sigma}_{cd}^{(0)}}{d\Phi_B} \lim_{\delta \rightarrow 0} e^{-\mathcal{R}_{\text{NLL}}(v)} \delta\mathcal{R}'_{\text{NLL}}(v) \sum_{n=0}^{\infty} \frac{1}{n!} \prod_{i=1}^n \int_{\delta}^1 \frac{d\zeta_i}{\zeta_i} \mathcal{R}'_{\text{NLL}}(v) \\ &\times \frac{\alpha_s(Qv^{\frac{1}{1+b}})}{\pi(1+b)} \int_{\delta}^1 \frac{d\zeta_{\text{hc}}}{\zeta_{\text{hc}}} \left(\sum_i \int_{x_c}^1 \frac{dz}{z} \hat{P}_{ci}^{(0)}(z) f_i\left(\frac{x_c}{z}, Qv^{\frac{1}{1+b}}\right) f_d\left(x_d, Qv^{\frac{1}{1+b}}\right) + \{c \leftrightarrow d\} \right) \\ &\times \left[\Theta(1 - \sum_i \zeta_i - \zeta_{\text{hc}}) - \Theta(1 - \zeta_{\text{hc}}) \Theta(1 - \sum_i \zeta_i) \right]. \end{aligned} \quad (3.22)$$

The above integrals can be evaluated by following the steps in Appendix C.3 of Ref. [88]. Finally, in the scale of the coupling and the PDFs we also expand the hard scale Q about the renormalisation and factorisation scales, respectively, which will allow us to estimate perturbative uncertainties via scale variations. We thus obtain, for $S_b^{(0)}$

$$\begin{aligned} \delta\Sigma_{\text{DGLAP}}^{pp}(v) &= -\frac{d\hat{\sigma}_{cd}^{(0)}}{d\Phi_B} e^{-\mathcal{R}_{\text{NLL}}(v)} \mathcal{F}_{\text{NLL}}(v) \frac{\alpha_s(\mu_R)}{\pi} \left(\psi^{(0)}(1 + \mathcal{R}'_{\text{NLL}}(v)) + \gamma_E \right) \frac{1}{1+b-2\lambda} \\ &\times \sum_i \left[(\hat{P}_{ci} \otimes f_i)(x_c, \mu_{\text{ISR}}) f_d(x_d, \mu_{\text{ISR}}) + \{c \leftrightarrow d\} \right], \end{aligned} \quad (3.23)$$

with μ_{ISR} given in Eq. (3.12). In practice, we evaluate Eq. (3.23) with the NNLL radiator $e^{-\mathcal{R}_{\text{NLL}}(v)} \rightarrow e^{-\mathcal{R}_{\text{NNLL}}(v)}$, which only introduces subleading, N^3LL corrections in our predictions for $S_b^{(0)}$.

3.2.1 Results for different reference frames

The formulas we have described so far in this section are valid if the observable is computed in the frame where the colour singlet has zero rapidity, which we refer to as the partonic

c.o.m. frame. However, it is also interesting to calculate such observables by defining the rapidity in the laboratory frame, that is in the c.o.m. frame of the colliding hadrons. It is easy to see that, at NLL accuracy, the two calculations are identical. At NNLL, we have three corrections, two of which are of soft origin. The first is a modification to the soft Sudakov radiator R_s^ℓ , defined in Eq. (3.4), whose expression is reported in Appendix A.2. This arises due to a change in the definition of the simple observable, which, in the case of the partonic c.o.m. frame, reads:

$$V_s^{(\ell)}(k_t^{(\ell)}, y^{(\ell)}) = \frac{k_t^{(\ell)}}{Q} e^{-b y^{(\ell)}}. \quad (3.24)$$

If we focus on the case in which $\ell = \ell_1$, i.e. radiation collinear to the beam aligned with the positive z -axis direction, the simple observable for the hadronic c.o.m. frame variant becomes

$$V_{s, \text{c.o.m.}}^{(\ell_1)}(k_t^{(\ell_1)}, y^{(\ell_1)}) = \lim_{y_{\text{c.o.m.}} \rightarrow +\infty} \frac{k_t^{(\ell_1)}}{Q} e^{-b|y_{\text{c.o.m.}}|} = e^{b y_F} \frac{k_t^{(\ell_1)}}{Q} e^{-b y^{(\ell_1)}}, \quad (3.25)$$

where $y_{\text{c.o.m.}}$ and y_F are the rapidity of the emission and of the colour singlet in the hadronic c.o.m. frame, and $y^{(\ell_1)} = y_{\text{c.o.m.}} - y_F$. Thus, we see that our simple observable now reads

$$V_{s, \text{c.o.m.}}^{(\ell)}(k_t^{(\ell)}, y^{(\ell)}) = d_\ell V_s^{(\ell)}(k_t^{(\ell)}, y^{(\ell)}), \quad \text{with } d_\ell = e^{\pm b y_F}, \quad (3.26)$$

where the $+$ ($-$) sign corresponds to ℓ_1 (ℓ_2). From Eq. (B.5) of Ref. [88], we observe that $g_2^{(\ell)}$ acquires a correction proportional to $\ln d_\ell$, which is equal and opposite in sign for both legs and hence disappears in the sum. Similarly, from Eq. (B.6) of the same reference, $g_3^{(\ell)}$ acquires a term proportional to $\ln d_\ell$, which also vanishes in the sum over legs. However, $g_3^{(\ell)}$ also contains a quadratic term⁷ that survives and amounts to the replacement $g_3^{(\ell)} \rightarrow g_3^{(\ell)} + \Delta g_3^{(\ell)}$, with

$$\begin{aligned} \Delta g_3^{(\ell)} &= -\frac{C_\ell}{(1-2\lambda)(1+b-2\lambda)} \ln^2 d_\ell = -\frac{2b^2 y_F^2 C_\ell}{(1-2\lambda)(1+b-2\lambda)} \\ &= -C_\ell b y_F^2 \frac{1}{\alpha_s(Q)} \left[\frac{\alpha_s(Q e^{-L/(1+b)})}{1+b} - \alpha_s(Q e^{-L}) \right]. \end{aligned} \quad (3.27)$$

The second contribution of soft origin arises from a wide-angle correction to the transfer function, hence contributing to $\delta \mathcal{F}_{\text{wa}}^{pp}$. This correction vanishes in the partonic c.o.m. frame (cf. comment in Appendix A.3), but it is non-zero in the hadronic c.o.m. frame. Indeed, assuming for simplicity that $y_F < 0$, we see that for leg ℓ_1 , in the region where $0 < y^{(\ell_1)} < y_F$, we have

$$V_{\text{wa, c.o.m.}}(k_t^{(\ell_1)}, y^{(\ell_1)}) = \frac{k_t^{(\ell_1)}}{Q} e^{-b|y^{(\ell_1)} - y_F|} = \frac{k_t^{(\ell_1)}}{Q} e^{+b(y^{(\ell_1)} - y_F)}, \quad (3.28)$$

⁷Strictly speaking, the $g_i^{(\ell)}$ of Ref. [88] are equal to $g_i^{(\ell)} + h_i^{(\ell)}$, i.e., they are the sum of the soft and collinear radiator. Hence, some of the terms linear in $\ln d_\ell$ would actually be in $h_3^{(\ell)}$ (i.e., the collinear radiator). The quadratic term, however, is of purely soft origin.

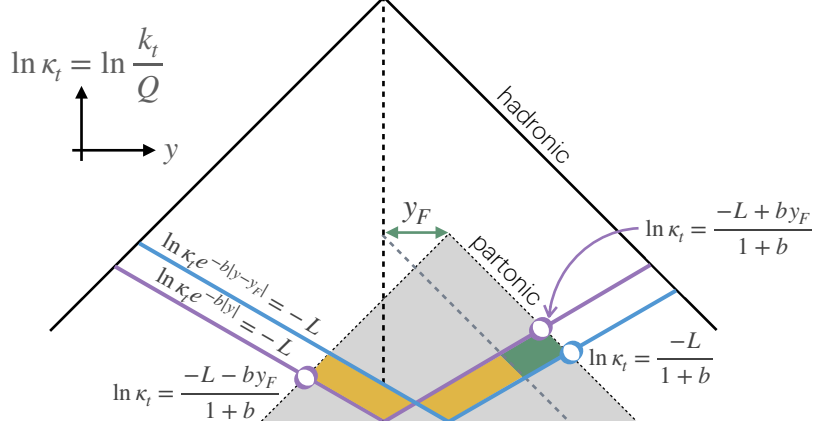


Figure 3: Location of NNLL corrections in the Lund plane when computing b -dependent LTS for pp events with rapidity defined in the event frame (purple) or in the frame where the colour singlet has zero rapidity (blue).

where the exponent has the opposite argument compared to the simple observable in Eq. (3.25). Starting from Eq. (C23) of Ref. [88] (which also applies to the $M_b^{(0)}$ observable), we can thus calculate this correction, obtaining

$$\begin{aligned}
 \delta \mathcal{F}_{\text{wa}}^{pp} &= - \sum_{\ell} \frac{2C_{\ell}\alpha_s(Q)}{\alpha_s(Qe^{-L})} \mathcal{F}_{\text{NLL}} \int_0^{\infty} dy^{(\ell)} \ln \frac{V_{\text{wa, c.o.m.}}}{V_{\text{s, c.o.m.}}} \\
 &= - \frac{2C_{\ell}\alpha_s(Qe^{-L})}{\alpha_s(Q)} \mathcal{F}_{\text{NLL}} \int_0^{y_F} dy^{(\ell_1)} 2b(y^{(\ell_1)} - y_F) \\
 &= 2C_{\ell} b y_F^2 \frac{\alpha_s(Qe^{-L})}{\alpha_s(Q)} \mathcal{F}_{\text{NLL}}. \tag{3.29}
 \end{aligned}$$

Combining the terms in Eqs. (3.27) and (3.29), we obtain that the total correction of soft origin is

$$\exp \left(-\frac{\alpha_s}{\pi} \sum_{\ell=\ell_1}^{\ell_2} \Delta g_3^{(\ell)} \right) \left(1 + \frac{\alpha_s}{\pi} \frac{\delta \mathcal{F}_{\text{wa}}^{pp}}{\mathcal{F}_{\text{NLL}}} \right) = 1 + \frac{\alpha_s(Qe^{-\frac{L}{1+b}})}{\pi} 2C_{\ell} b y_F^2 + \mathcal{O}(N^3 \text{LL}). \tag{3.30}$$

Notice that this term could also have been obtained from a geometric argument, as it corresponds to the Lund plane density integrated over the green region of Fig. 3. Indeed, it can be naively interpreted as the amount of soft-collinear radiation that is included in the Sudakov radiator for the partonic c.o.m. frame observable, and needs to be removed for the hadronic c.o.m. frame case. One sees in Fig. 3 that the contributions form the two yellow shaded areas cancel each other, so that the difference is given by the green shaded area. This area has no logarithmic enhancement and is therefore relevant at the NNLL accuracy. This argument also shows the appearance of $Qe^{-\frac{L}{1+b}}$ as the scale at which α_s has to be evaluated.

Finally, we examine the last correction, which is of hard-collinear origin. This arises from the fact that the collinear scale μ_{ISR} , at which the PDF needs to be evaluated (rep-

resented by empty dots in Fig. 3), now receives a small modification:

$$\ln \frac{\mu_{\text{ISR}}}{Q} = \frac{-L}{1+b} \rightarrow \frac{-L \pm b y_F}{1+b}, \quad (3.31)$$

where the $+$ ($-$) sign applies to the incoming parton with positive (negative) rapidity. At NNLL accuracy, this results in the following replacement in the scale of the parton densities in Eqs. (3.10), (3.23)

$$f_\ell \left(x, \mu_F e^{-\frac{L}{1+b}} \right) \rightarrow f_\ell \left(x, \mu_F \exp \left(\frac{-L - (-1)^\ell b y_F}{1+b} \right) \right), \quad (3.32)$$

where we conventionally choose the beam $\ell = \ell_1$ to be in the positive-rapidity hemisphere. Eq. (3.23) is then expanded around the scale $\mu_F e^{-\frac{L}{1+b}}$ using the DGLAP equation, neglecting contributions beyond NNLL.

The sum of all contribution derived above could be alternatively collected into a correction to the result in the partonic c.o.m. frame in Eq. (3.14), that reads

$$\begin{aligned} \delta\Sigma_{\text{frame}}^{pp}(v, \Phi_B) &= \frac{d\hat{\sigma}_{cd}^{(0)}}{d\Phi_B} e^{-\mathcal{R}_{\text{NNLL}}(v)} \mathcal{F}_{\text{NLL}}(v) \frac{b y_F}{1+b-2\lambda} \frac{\alpha_s(\mu_R)}{\pi} \\ &\times \left[2C_\ell y_F f_c(x_c, \mu_F e^{-\frac{L}{1+b}}) f_d(x_d, \mu_F e^{-\frac{L}{1+b}}) \right. \\ &\left. + \sum_i \left((\hat{P}_{ci} \otimes f_i)(x_c, \mu_F e^{-\frac{L}{1+b}}) f_d(x_d, \mu_F e^{-\frac{L}{1+b}}) - \{c \leftrightarrow d\} \right) \right]. \end{aligned} \quad (3.33)$$

3.2.2 Absence of non-global logarithms in the multi-jet case

In this section, we discuss the absence of non-global logarithms [93–99] in the resummation of LTS, in particular when three or more coloured legs are present already at the Born level. For the sake of arguments, we examine one such processes, $pp \rightarrow Fj$, where F is a generic colour singlet and j is a hard and resolved final-state jet. We then start by performing a fixed-order calculation of the leading non-global configuration, stemming from the emission of a pair of soft wide-angle gluons with momentum $p_{1,2}$ strongly ordered in energy. At this order, non-global corrections arise from scenarios in which one of the two gluons propagates inside the jet j and one propagates outside (and hence clusters with the beam in the definition of the LTS). We introduce the following parameterisation for the kinematics

$$\begin{aligned} p_n &= E_n(1, 0, 0, 1), \quad p_{\bar{n}} = E_{\bar{n}}(1, 0, 0, -1), \\ p_\ell &= p_{t,\ell}(\cosh \eta_\ell, \sin \phi_\ell, \cos \phi_\ell, \sinh \eta_\ell), \quad \ell \in \{j, 1, 2\}, \end{aligned} \quad (3.34)$$

where $p_{n,\bar{n}}$ denote the momenta of the two incoming partons and p_j that of the final-state jet, and all quantities are defined w.r.t. the beam axis. To simplify the calculation, we work in the planar, large- N_c limit ($C_F = C_A/2 = N_c/2$) that is customary in the study of non-global observables. The Born will be then a collection of dipoles. To single out the

leading non-global configuration, we consider the situation in which the two emissions are strongly ordered and we write the corresponding emission probability as

$$\begin{aligned} [dp_1][dp_2]W_2 &= [dp_1][dp_2](4\pi\alpha_s)^2 N_c^2 \sum_{\{ik\} \in \text{dipoles}} \frac{(ik)}{(i1)(k1)} \left(\frac{(i1)}{(12)(i2)} + \frac{(k1)}{(12)(k2)} - \frac{(ik)}{(i2)(k2)} \right) \\ &\equiv 4(4\pi\alpha_s)^2 N_c^2 \frac{[dp_1][dp_2]}{p_{t,1}^2 p_{t,2}^2} w_2, \end{aligned} \quad (3.35)$$

where

$$[dp_i] = \frac{d\eta_i}{2} \frac{p_{t,i} dp_{t,i} d\phi_i}{(2\pi)^3}, \quad (3.36)$$

and we adopted the notation $(ij) \equiv p_i \cdot p_j$. In Eq. (3.35), we have subtracted the primary contribution to the squared amplitude, which is a source of double logarithmic corrections and has been already accounted for in our resummation. To parameterise the phase space, we perform the change of variables

$$v_i = p_{t,i} e^{-b|\eta_i|}, \quad \eta_i - \eta_j = R r_i \cos \theta_i, \quad \phi_i - \phi_j = R r_i \sin \theta_i \quad \text{with } i = 1, 2 \quad (3.37)$$

for which the phase-space factor reads

$$4(4\pi\alpha_s)^2 N_c^2 \frac{[dp_1][dp_2]}{p_{t,1}^2 p_{t,2}^2} = \left(\frac{\alpha_s}{\pi} \right)^2 N_c^2 \frac{R^4}{(4\pi)^2} \prod_{i=1,2} \frac{dv_i}{v_i} dr_i^2 d\theta_i. \quad (3.38)$$

With these definitions, the clustering condition for a parton p_i to be recombined with the jet p_j is

$$d_{j,i}^2 = r_i^2 R^2 < R^2. \quad (3.39)$$

Requiring that only one of the two radiated particles clusters then leads to the following two possible angular constraints

$$\Theta_A = \Theta(r_1 - 1)\Theta(1 - r_2)\Theta(r_1 - 2r_2 \cos(\theta_1 - \theta_2)), \quad p_1 \text{ out, } p_2 \text{ in} \quad (3.40a)$$

$$\Theta_B = \Theta(1 - r_1)\Theta(r_2 - 1)\Theta(r_2 - 2r_1 \cos(\theta_1 - \theta_2)), \quad p_1 \text{ in, } p_2 \text{ out} \quad (3.40b)$$

where the last Θ function enforces that the two particles $p_{1,2}$ are not clustered first. In the strongly ordered limit $v_1 \gg v_2$, non-global logarithms arise [93] if the following phase-space integral

$$\begin{aligned} &\left(\frac{\alpha_s}{\pi} \right)^2 N_c^2 \frac{R^4}{(4\pi)^2} \int \prod_{i=1}^2 dr_i^2 d\theta_i w_2(\{r_i, \theta_i\}) \\ &\quad \times \int_0^\infty \frac{dv_1}{v_1} \int_0^\infty \frac{dv_2}{v_2} (\Theta(v - V(p_1, p_2)) - \Theta(v - V(p_1))) \Theta_{A/B} \Theta(v_1 - v_2) \end{aligned} \quad (3.41)$$

develops logarithmic terms $\mathcal{O}(\ln^n(v))$. The second term in Eq. (3.41) corresponds to the virtual correction, which in the strongly ordered limit can be approximated by simply imposing unitarity. Moreover, $\Theta(v_1 - v_2)$ is the (strong) ordering condition. Due to the

way we parameterise the phase space, we can focus only on the $v_{1,2}$ integration to assess the presence of a logarithmically-enhanced term.

It is now straightforward to see that, when $v_1 \gg v_2$, we have $V(p_1, p_2) = V(p_1) \neq 0$, so that no non-global logarithm can arise from the above integral. This is a direct consequence of the fact that the observable resolves the substructure of jets, hence imposing a commensurate constraint over all emissions regardless of whether they cluster with the beam or with the jet. To be explicit, let us consider case *A*, where only p_2 clusters with the final-state jet. In the case of the LTS in this process (cf. Section 2.2), the first emission contributes with v_1 , whereas the second emission contributes with

$$p_{t,2} e^{-b|\eta_j|} r_2^{1+b} = v_2 r_2^{1+b} e^{-b(|\eta_j|-|\eta_2|)} \equiv v_2 g(r_2, \theta_2). \quad (3.42)$$

For $S_b^{(1)}$ and $M_b^{(1)}$, we thus have $V(p_1) = v_1$ and

$$V(p_1, p_2) = \begin{cases} v_1 \max \left\{ 1, \frac{v_2}{v_1} g(r_2, \theta_2) \right\} & \text{for } M_b^{(1)} \\ v_1 \left(1 + \frac{v_2}{v_1} g(r_2, \theta_2) \right) & \text{for } S_b^{(1)} \end{cases}. \quad (3.43)$$

We therefore find that the integral is given by

$$\begin{aligned} \int_0^v \frac{dv_1}{v_1} \int_0^{v_1} \frac{dv_2}{v_2} [\Theta(v - V(p_1, p_2)) - \Theta(v - V(p_1))] &= \\ &= \begin{cases} -\frac{1}{2} \ln^2(\max \{1, g(r_2, \theta_2)\}) & \text{for } M_b^{(1)} \\ \text{Li}_2(-g(r_2, \theta_2)) & \text{for } S_b^{(1)} \end{cases}, \end{aligned} \quad (3.44)$$

which is free of logarithmic terms. An analogous conclusion holds for case *B*, in which p_1 clusters with the jet and p_2 clusters with the beam. The remaining angular integral is of $\mathcal{O}(1)$ as long as $R \sim \mathcal{O}(1)$, which proves the absence of non-global logarithms at this perturbative order.

Our conclusions readily extend to all perturbative orders (both in α_s and in the resummation). The mechanism that led to the cancellation of non-global logarithms in the above example relies on the recursive nature of the observable that resolves the structure of radiation inside the jet. As a result, for any number of emissions $\{p_i\}$, the observable scales uniformly across different regions of the solid angle, that is $V(\{p_i\}) \sim V(p_j) \sim v$ where p_j is any one of the $\{p_i\}$ emissions, as long as $R \sim \mathcal{O}(1)$. This guarantees that all phase-space configurations that would typically lead to non-global logarithms now give at most a non-logarithmic contribution to the observable whose coupling is evaluated at the soft scale $Q e^{-L}$. In practice, this means that beyond NNLL, the extension of the wide-angle function $\delta\mathcal{F}_{\text{wa}}$ will receive contributions involving the non-trivial clustering of emissions near the jet boundary, all at commensurate scales of order $Q e^{-L}$.

3.2.3 Comment on possible coherence-violating effects at higher orders

Although our observables are free of non-global logarithms at all logarithmic orders, their logarithmic structure in the pp case may be affected by coherence-violating corrections at higher-loop orders. Such corrections appear beyond the leading- N_c level and originate from

Glauber gluons exchanges. They are known to be present in global observables that are not sufficiently inclusive over final-state radiation [7, 100–103].⁸ These studies indicate that such coherence-violating corrections might as well appear in the case of LTS at sufficiently high perturbative orders. We do not consider these corrections here and leave their study to future work.

3.3 $N = 1$ case in DIS

We now consider the LTS at lepton-hadron colliders, $\Sigma^{ep}(v)$. The resummation of the simple observable $\Sigma_S^{ep}(v)$ can be obtained from the ingredients of the lepton- ($\Sigma_S^{ee}(v)$) and hadron-collider ($\Sigma_S^{pp}(v)$) cases given in Eq. (3.3) and Eq. (3.10), respectively. We label the flavour of the incoming parton by c and that of the outgoing parton by d . The resummation for $\Sigma_S^{ep}(v, \Phi_B)$ reads

$$\Sigma_S^{ep}(v, \Phi_B) = \frac{d\hat{\sigma}_{cd}^{(0)}}{d\Phi_B} \exp\{-\mathcal{R}_{\text{NNLL}}(v)\} \left[f_c(x_1, \mu_{\text{ISR}}) \left(1 + \frac{\alpha_s(\mu_R)}{2\pi} H_{cd}^{(1)}(\Phi_B) \right) + \frac{\alpha_s(\mu_R)}{2\pi} \frac{1+b}{1+b-2\lambda} \left(\sum_i (C_{ci}^{(1)} \otimes f_i)(x_1, \mu_{\text{ISR}}) + f_c(x_1, \mu_{\text{ISR}}) C_{\text{hc},d}^{(1)} \right) \right], \quad (3.45)$$

where the hard-collinear constant $C_{\text{hc},d}^{(1)}$ depends on whether the flavour d is a gluon or a quark. The resummation for the cumulative cross section for the ep case follows from the ee and pp cases, and takes the form

$$\Sigma^{ep}(v, \Phi_B) = \Sigma_S^{ep}(v, \Phi_B) \mathcal{F}^{ep}(v) + \delta\Sigma_{\text{DGLAP}}^{ep}(v, \Phi_B), \quad (3.46)$$

with

$$\mathcal{F}^{ep}(v) = \mathcal{F}_{\text{NLL}}^{ep}(v) + \frac{\alpha_s(\mu_R)}{\pi} \delta\mathcal{F}_{\text{NNLL}}^{ep}(v), \quad (3.47)$$

and

$$\mathcal{F}_{\text{NLL}}^{ep}(v) = \mathcal{F}_{\text{NLL}}^{pp}(v) = \mathcal{F}_{\text{NLL}}^{ee}(v), \quad (3.48)$$

$$\mathcal{F}_{\text{NNLL}}^{ep}(v) = \delta\mathcal{F}_{\text{sc}}^{ep}(v) + \delta\mathcal{F}_{\text{wa}}^{ep}(v) + \delta\mathcal{F}_{\text{correl}}^{ep}(v) + \delta\mathcal{F}_{\text{clust}}^{ep}(v) + \delta\mathcal{F}_{\text{hc}}^{ep}(v) + \delta\mathcal{F}_{\text{rec}}^{ep}(v). \quad (3.49)$$

The expressions for all the ingredients are given in Appendix A. As in the pp case, the DGLAP correction $\delta\Sigma_{\text{DGLAP}}^{ep}(v, \Phi_B)$ is absent for $M_b^{(1)}$ and for $S_b^{(1)}$ it reads

$$\begin{aligned} \delta\Sigma_{\text{DGLAP}}^{ep}(v) = & - \frac{d\hat{\sigma}_{cd}^{(0)}}{d\Phi_B} \exp\{-\mathcal{R}_{\text{NNLL}}(v)\} \mathcal{F}_{\text{NLL}}^{ep}(v) \frac{\alpha_s(\mu_R)}{\pi} \left(\psi^{(0)}(1 + \mathcal{R}'_{\text{NLL}}(v)) + \gamma_E \right) \\ & \times \frac{1}{1+b-2\lambda} \sum_i (\hat{P}_{ci} \otimes f_i)(x_1, \mu_{\text{ISR}}). \end{aligned} \quad (3.50)$$

Notice that, unlike for the pp case, now both the DGLAP and the recoil corrections contribute, due to the presence of emitting partons both in the initial and final state.

⁸Corresponding studies of coherence-violating corrections in non-global observables can be found, e.g., in Refs. [104–115].

3.4 Fixed-order validation up to second perturbative order for pp

In this section we discuss the validation of our resummation for the LTS. As a first check, we compare the expansion of our resummation in powers of α_s to an exact fixed-order calculation. We recall that NNLL resummation implies control, at the cumulative level, over the terms $\alpha_s L^2, \alpha_s L, \alpha_s$ (i.e. all terms at NLO in the small- v limit), as well as $\alpha_s^2 L^4, \dots, \alpha_s^2 L$ (i.e. all but the $\mathcal{O}(\alpha_s^2 L^0)$ term at NNLO). Therefore, we consider the difference between the fixed-order (fo) and resummed-expanded (res) predictions at the differential level, namely,

$$\Delta f^{(i)}(v) \equiv \frac{1}{\sigma^{(0)}} \left[\frac{d\Sigma_{\text{fo}}^{(i)}}{d \ln v} - \frac{d\Sigma_{\text{res}}^{(i)}}{d \ln v} \right], \quad (3.51)$$

where

$$\Sigma_{\text{res}} = \sum_{i=0}^2 \Sigma_{\text{res}}^{(i)} + \mathcal{O}(\alpha_s^3 \sigma^{(0)}), \quad \Sigma_{\text{fo}} = \sum_{i=0}^2 \Sigma_{\text{fo}}^{(i)}. \quad (3.52)$$

As a function of $L = -\ln(v)$, we expect that $\Delta f^{(i)}(v) \rightarrow 0$ for small v and $i = 1, 2$. Note that the correctness of the NLO term $\mathcal{O}(\alpha_s L^0)$ in our resummation is tested in the $\mathcal{O}(\alpha_s^2)$ check for $\Delta f^{(2)}(v)$.

The fixed-order reference results are obtained from `Event2` [116] (for ee), `disorder` [116–118] (for ep) and `Matrix` [119] (for pp). Here we will only show our validations for $pp \rightarrow Z$ and $pp \rightarrow H$, while those for ee and ep are collected in Appendix C. The phenomenological setup for obtaining the fixed-order and resummed-expanded result is the same as the one used to obtain our final results, and will be detailed in Sec. 4.2. For our test we consider central scales, $\mu_F = \mu_R = Q$, where Q is the mass of the Z or Higgs boson, with $M_Z = 91.1976$ GeV and $M_H = 125$ GeV.

The results are shown in Fig. 4. In the top panel we show the NLO comparison for $S_b^{(0)}$ and $M_b^{(0)}$, which are the same at this order since there can be at most one emission. We observe, as expected, that $\Delta f^{(1)}(v)$ vanishes in the limit $v \rightarrow 0$ for the values of b considered ($b = 0, 1/2$ and $b = 1$). The remaining panels show the NNLO results. We see that the NNLO convergence is slightly slower, as shown in the middle ($M_b^{(0)}$) and bottom ($S_b^{(0)}$) panels of Fig. 4, as the power corrections will be enhanced by additional logarithms. For large values of $-\ln v$, we observe the expected agreement between the fixed-order and the expanded resummed predictions. In Fig. 4, we observe that the $b = 0$ results converge to their asymptotic values for larger values of v than for the $b = 1/2$ and $b = 1$ cases, which is directly related to the structure of their power corrections as well as the different dependence on the radiation rapidity in the three cases. Note, however, that the computational cost to reach the asymptotic region of convergence is comparable for different b values, as it is also reflected on the size of the statistical errors at lower values of v . Interestingly, we note that, within the same b and at order $\mathcal{O}(\alpha_s^2)$, there is a mildly faster convergence for $M_b^{(0)}$ than for $S_b^{(0)}$, which deserves further investigations on the size of their power corrections.

We performed additional tests to validate the dependence on the renormalisation (μ_R), factorisation (μ_F) and resummation (μ_L , cf. Eq. (4.1)) scales of our predictions. Firstly,

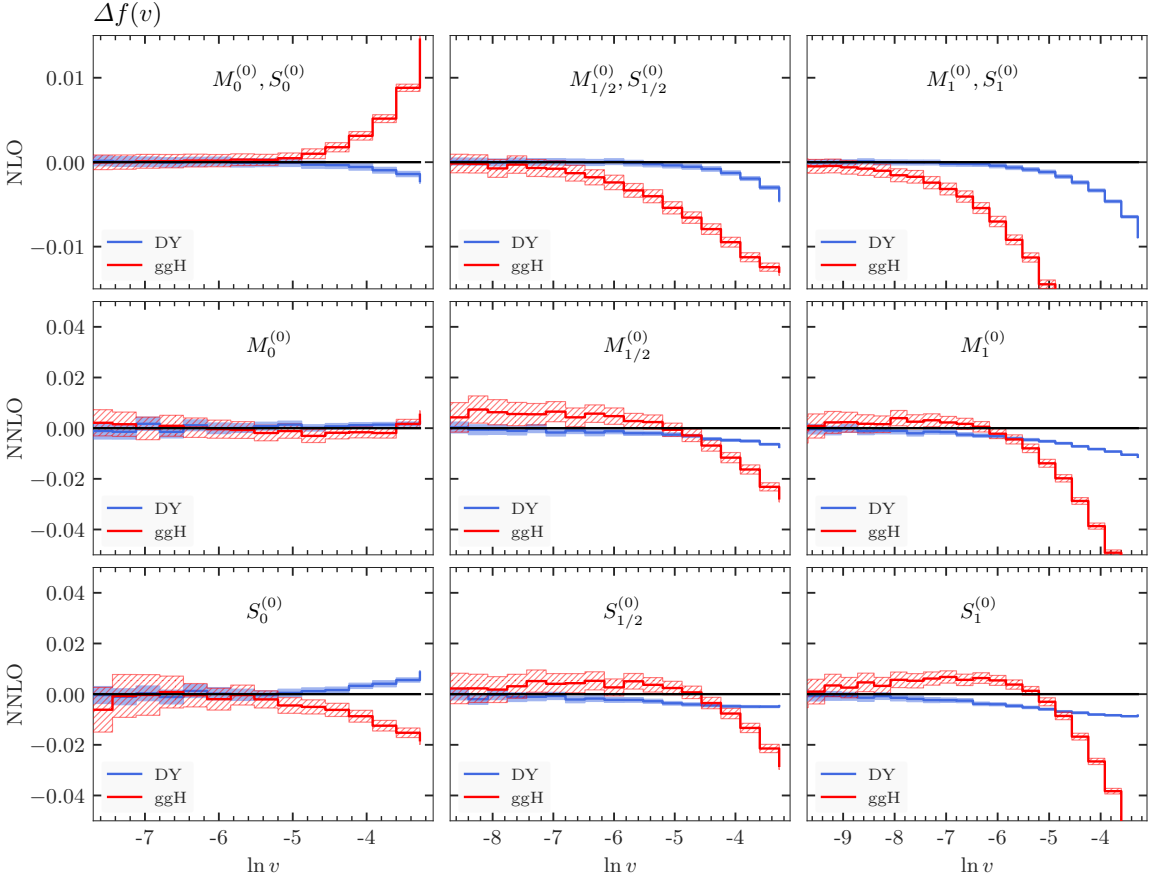


Figure 4: Difference between the fixed-order and resummed-expanded differential cross sections, normalised to the Born cross section, c.f. Eq. (3.51), for DY (blue) and gluon fusion Higgs (red) production. We consider three values of b , $b = 0$ (left), $b = 1/2$ (middle) $b = 1$ (right). The top panel shows the NLO comparison for $S_b^{(0)}/M_b^{(0)}$. The middle (bottom) panel shows the NNLO comparison for $M_b^{(0)}$ ($S_b^{(0)}$). The bands show the statistical uncertainty.

we have verified the correctness of the scale dependence up to relative order $\mathcal{O}(\alpha_s^2)$ by repeating the comparison of the expansion of the resummation and the fixed order results for individual scale variations. In all cases, we find results similar to those reported in Fig. 4 for central scales. Secondly, we checked that the μ_R, μ_F dependence of our NNLL result exactly cancels at relative order $\mathcal{O}(\alpha_s^2)$, while their dependence amounts to an $\mathcal{O}(\alpha_s^3 L)$ effect. This is done numerically through the evaluation of our NNLL expressions and their expansion at a small values of α_s . In addition, we checked that the μ_L dependence starts at $\mathcal{O}(\alpha_s^2 L^0)$, which is expected since we have not included $\mathcal{O}(\alpha_s^2)$ constants in our resummed result.

4 NNLL+NNLO predictions and Monte Carlo studies for the LHC

In this section, we discuss some phenomenological considerations for the LTS, including the matching of our resummed predictions to NNLO fixed-order results at the cumulative cross-section level, as well as the impact of non-perturbative corrections (i.e. hadronisation) and underlying event.

4.1 Matching to fixed order

We now discuss the matching of our resummed predictions to a fixed order, NNLO calculation. We will consider the pp case, although an analogous procedure can be used for the ee and ep cases. Similarly, the extension to higher orders is straightforward.

To perform the matching, we first need to ensure that at large v , the resummation is turned off. Furthermore, we want to have a handle on the size of subleading logarithmic corrections in the resummation, to be included in the estimate of theoretical uncertainties. We proceed in two steps. Firstly, we split the resummed logarithm as

$$\ln \frac{1}{v} = \ln \frac{\mu_L}{Qv} + \ln \frac{Q}{\mu_L} = L + \ln \frac{Q}{\mu_L}, \quad (4.1)$$

and then we expand the dependence in the resummed prediction on the second term ($\ln \frac{Q}{\mu_L}$) by truncating the expansion at NNLL, hence inducing a dependence on μ_L that is strictly N³LL. As a consequence all the ingredients of the resummation will depend on μ_L , and their corresponding expressions are provided in Appendix A. The scale μ_L is the *resummation scale*, which we will vary around Q to estimate the size of subleading logarithms in the prediction. As a second step, we now modify μ_L and L as follows⁹

$$\mu_L \rightarrow \bar{\mu}_L(v) = \begin{cases} \mathfrak{r}(v) & \text{for } v < v_M, \\ \mathfrak{m}(v) & \text{for } v_M \leq v < 1, \\ Q & \text{for } v \geq 1, \end{cases} \quad (4.2)$$

and

$$L \rightarrow L \Theta \left(\frac{\mu_M}{Q} - v \right). \quad (4.3)$$

The functions $\mathfrak{r}(v)$ and $\mathfrak{m}(v)$ are polynomials in the (dimensionless) observable v , whose expressions are given in Appendix B, where more information is provided. They guarantee continuity of both the cumulative and differential distributions for $v = v_M$ and $v = 1$. The logarithm L is now switched off at $v = v_M = \mu_M/Q \leq 1$, where μ_M is a *matching scale*, to be taken of order Q .

To match the NNLO fixed-order and NNLL resummed results, we will use a multiplicative matching scheme inspired to those introduced in Refs. [9, 13, 120, 122]. We introduce the notation for the fixed-order expansions of the ingredients up to relative order $\mathcal{O}(\alpha_s^2)$

⁹In the past, this was achieved by modifying the definition of the logarithm $L \rightarrow \tilde{L} = \frac{1}{p} \ln \left(1 + \left(\frac{\mu_L}{Qv} \right)^p \right)$, see e.g. Refs. [9, 13, 92, 120]. Instead, here we adopt a dynamical resummation scale, similar in spirit to what was done in Ref. [121].

w.r.t. the Born, working at the level of the integrated, cumulative cross section with any phase space cuts on the Born kinematics Φ_B and a veto v on the resolution variables studied here. We denote the fiducial cross section with any phase space cuts on the Born phase space Φ_B by σ_{fid} ($\sigma_{\text{fid}} = \sigma_{\text{total}}$ if no cuts are applied) and define, in addition to Eq. (3.52),

$$\sigma_{\text{fid}} = \sum_{i=0}^2 \sigma_{\text{fid}}^{(i)}, \quad \Sigma_{\text{fo}}(v) = \sum_{i=0}^2 \Sigma_{\text{fo}}^{(i)}(v) = \sigma_{\text{fid}} - \sum_{i=1}^2 \bar{\Sigma}_{\text{fo}}^{(i)}(v), \quad (4.4a)$$

$$\Sigma_{L \rightarrow 0} = \Sigma_{\text{res}}(v)|_{L \rightarrow 0} = \sigma_{\text{fid}}^{(0)} + \sum_{i=1}^2 \Sigma_{L \rightarrow 0}^{(i)}, \quad (4.4b)$$

where $\Sigma_{\text{fo}}(v)$ ($\bar{\Sigma}_{\text{fo}}(v)$) is the cumulative fixed-order cross section below (above) the cut v , and Σ_{res} is its resummed analogue, that is

$$\Sigma_{\text{res}}(v) = \int_{\text{cuts}} d\Phi_B \Sigma^{pp}(v, \Phi_B), \quad (4.5)$$

where the integral is performed taking into account any cuts on the Born kinematics. The quantity $\Sigma_{L \rightarrow 0}$ is obtained by setting $L = 0$ in the resummed prediction. We stress that, in general, $\ln Q/\mu_L \neq 0$ (cf. Eq. (4.1) and discussion thereof) in $\Sigma_{L \rightarrow 0}$. The matched cross section can be written as

$$\begin{aligned} \Sigma_{\text{mat}}(v) = & \frac{\Sigma_{\text{res}}(v)}{\Sigma_{L \rightarrow 0}} \left[\Sigma_{L \rightarrow 0} + \Sigma_{\text{fo}}^{(1)}(v) - \Sigma_{\text{res}}^{(1)}(v) \right. \\ & \left. + \Sigma_{\text{fo}}^{(2)}(v) - \Sigma_{\text{res}}^{(2)}(v) + \left(\frac{\Sigma_{L \rightarrow 0}^{(1)}}{\sigma_{\text{fid}}^{(0)}} - \frac{\Sigma_{\text{res}}^{(1)}(v)}{\sigma_{\text{fid}}^{(0)}} \right) \left(\Sigma_{\text{fo}}^{(1)}(v) - \Sigma_{\text{res}}^{(1)}(v) \right) \right]. \end{aligned} \quad (4.6)$$

The advantage of a multiplicative matching scheme like the one in Eq. (4.6) is that terms $\mathcal{O}(\alpha_s^2 L^0)$, formally of N^3LL order, are recovered correctly from the matching, effectively promoting the accuracy of the prediction to what is commonly labelled as $NNLL' + NNLO$.

4.2 Results at the LHC

In this section we report our predictions for $M_b^{(0)}$ and $S_b^{(0)}$ in neutral-current DY production. We consider pp collisions at a centre-of-mass energy of 13 TeV and use the `NNPDF40MC_nnlo_as_01180` [123] PDF set. The required convolutions with the PDFs are handled with the `Hoppet` package [118, 124], whereas the parton densities themselves are evaluated via `LHAPDF` [125]. Note that NNLO DGLAP evolution of the PDF set is used for our results, even though this level of evolution is of N^3LL order. We require that the Z boson is exactly on-shell with a mass of $Q = M_Z = 91.1976$ GeV. We use the C/A algorithm to cluster the event, and take $R = 0.8$ as our jet radius. The choice of the large jet radius is motivated by the fact that it increases the sensitivity to underlying events, which we wish to examine below. Smaller values of R are on the other hand preferable for phenomenological applications. We assess the missing higher-order uncertainties by performing a 7-point scale variation of μ_R and μ_F by a factor of two around their central values $\mu_R = \mu_F = Q$. In addition, we vary the resummation scale μ_L by a factor of 2 around

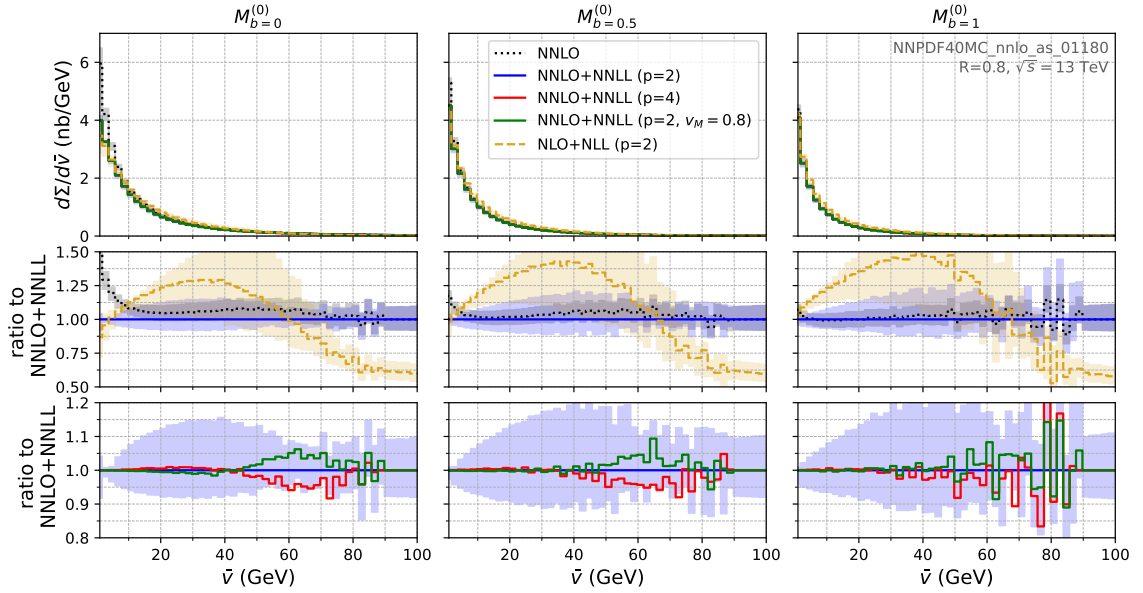


Figure 5: Differential distribution for $M_b^{(0)}$ with $b = 0$ (left), $b = 1/2$ (middle) and $b = 1$ (right) as a function of $\bar{v} = v Q$. The black dotted curve represents the NNLO result, the yellow dashed curve the NLO+NLL result, the blue (red) solid curve the NNLL+NNLO result with $p = 2$ ($p = 4$) in Eq. (4.2). The green curve shows the NNLL+NNLO result with $p = 2$ and $v_M = 0.8$. Scale uncertainties (computed as explained in the text) are indicated via the opaque bands. The middle panel shows the ratio of the NLO+NLL and NNLO results with respect to the NNLL+NNLO with $p = 2$ ($v_M = 1$) result. The bottom panel shows the ratio of the NNLO+NNLO result with $p = 4$ and that with $p = 2$ and $v_M = 0.8$ to the $p = 2$, $v_M = 1$ result.

$\mu_L = Q$, for the central choice of μ_R, μ_F . The resulting uncertainty is taken as the envelope of these 9 different scale variations. In our dynamical resummation scale (cf. Appendix B) we use $q = p$ and set the default value to $p = 2$. To assess the matching uncertainties we also consider the predictions with $p = 4$ and, separately, with a variation of the matching scale from $\mu_M = Q$ to $\mu_M = 0.8 Q$. The fixed-order results are obtained from **Matrix** [119].

In Fig. 5 we show the differential distributions for $M_b^{(0)}$ with $b = 0, 1/2$ and 1 at various levels of accuracy, with the band representing the perturbative uncertainty as outlined above. To avoid confusion, we stress that the fixed-order accuracy for the differential distributions is actually one order down w.r.t. that of the cumulative counterpart, i.e. a NNLO cumulative cross section corresponds to a NLO differential distribution. To show the scales probed by the observables in the plots, we display a dimensionful version $\bar{v} \equiv v Q$ on the x axis. One clearly sees the effect of the resummation becoming relevant at low values of \bar{v} , while the matched curves tend to the fixed-order result around $\bar{v} \sim \mu_M$, as guaranteed by the form of the resummation scale μ_L given in Eq. (4.2). The perturbative uncertainties are significantly reduced by going from NLL+NLO to NNLL+NNLO, and the two uncertainty bands of the two predictions show a good degree of overlap at small \bar{v} ,

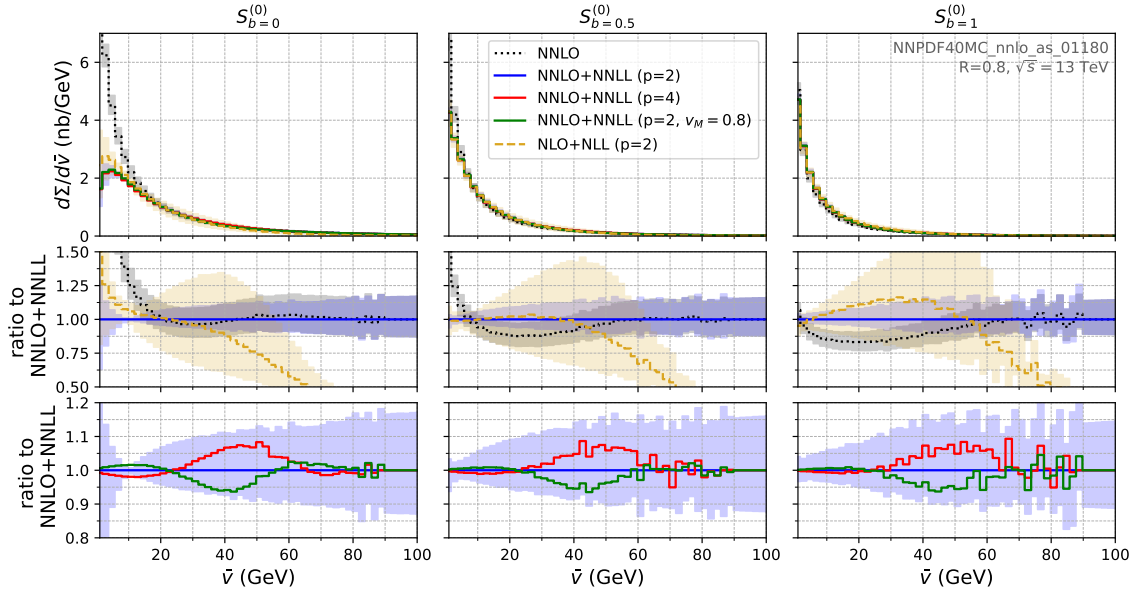


Figure 6: Same as Fig. 5 but for $S_b^{(0)}$.

indicating the robustness of the error estimates. At larger values of \bar{v} , where the prediction is given by the fixed order, the large difference between the NLO and NNLO predictions is representative of the fact that the former is only LO accurate for the \bar{v} spectrum, and hence subject to large radiative corrections captured by the higher-order predictions. As a further check of the stability of our matching procedure, we also show the prediction with a different value for p in Eq. (4.2) ($p = 4$), as well as the prediction with $\mu_M = 0.8 Q$. This does not affect, by design, the distributions for $\bar{v} \rightarrow 0$ and has the effect of shifting mildly the central value in the matching region $\bar{v} \sim \mu_M$, above which the matched curves reproduce the fixed-order result. The predictions obtained with these variations are contained within the error band, suggesting that the matching uncertainties are under control. Quantitatively similar features can be seen for $S_b^{(0)}$ shown in Fig. 6. Furthermore, Figs. 7, 8 show analogous predictions at the cumulative cross-section level.

4.3 Impact of multi-parton scattering and hadronisation

We now study the impact of hadronisation and underlying event on the LTS. We do so by performing `Pythia8.3` [126] simulations for $pp \rightarrow Z$ at 13 TeV. We keep the width of the Z -boson fixed to a small value so as to mimic the on-shell condition used in our perturbative calculations. All other parameters, including the jet clustering settings and the chosen PDF set are the same as in the previous section. We perform the study at the level of the cumulative distributions since they are more relevant to phenomenological applications of the LTS as jet vetoes. All distributions are now normalised by the total cross section, which coincides with the Born cross section in the `Pythia8.3` simulations.

The results for $M_b^{(0)}$ are shown in Fig. 9. We observe that hadronisation corrections remain below 5% across the region of $M_b^{(0)}$ relevant for experimental analyses, i.e. $Q M_b^{(0)} >$

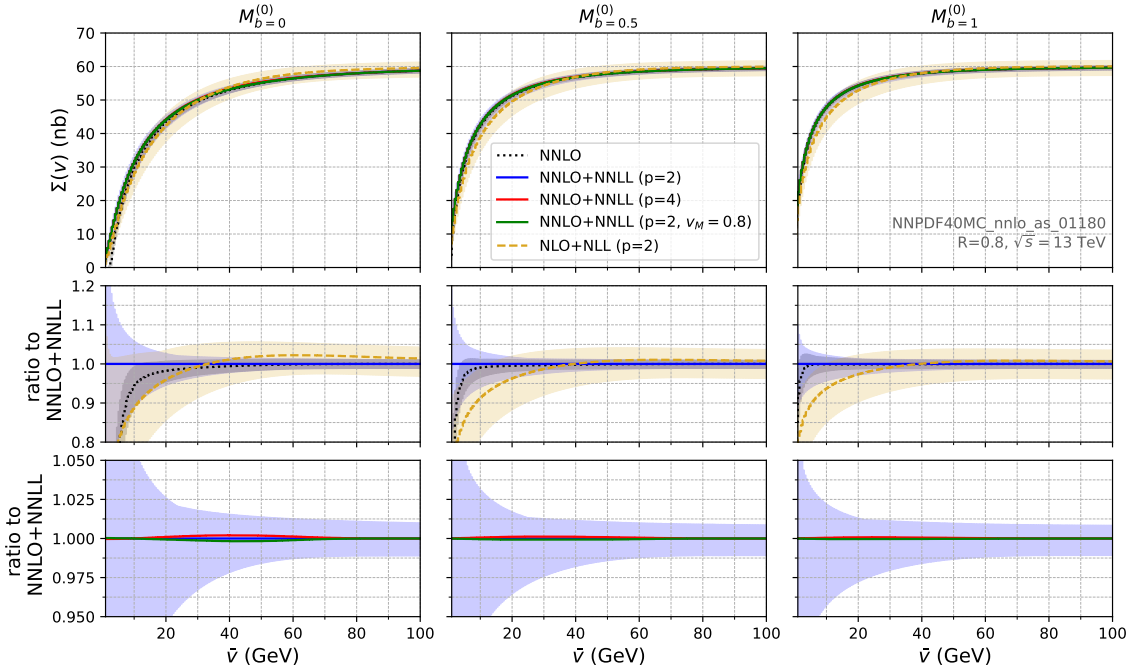


Figure 7: Same as Fig. 5 but for the cumulative distribution.

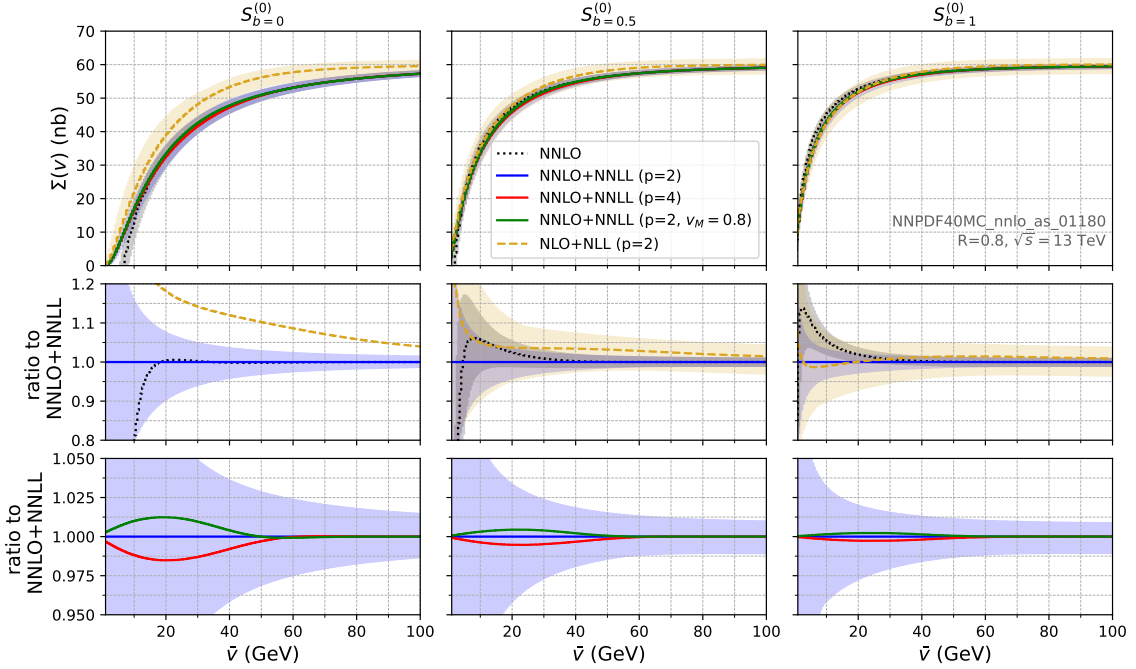


Figure 8: Same as Fig. 7 but for $S_b^{(0)}$.

10 GeV. In turn, multi-parton interactions (MPI) lead to a sizeable correction, up to 50% at $Q M_b^{(0)} = 10$ GeV for all values of b , but they are reduced swiftly as the value of $M_b^{(0)}$

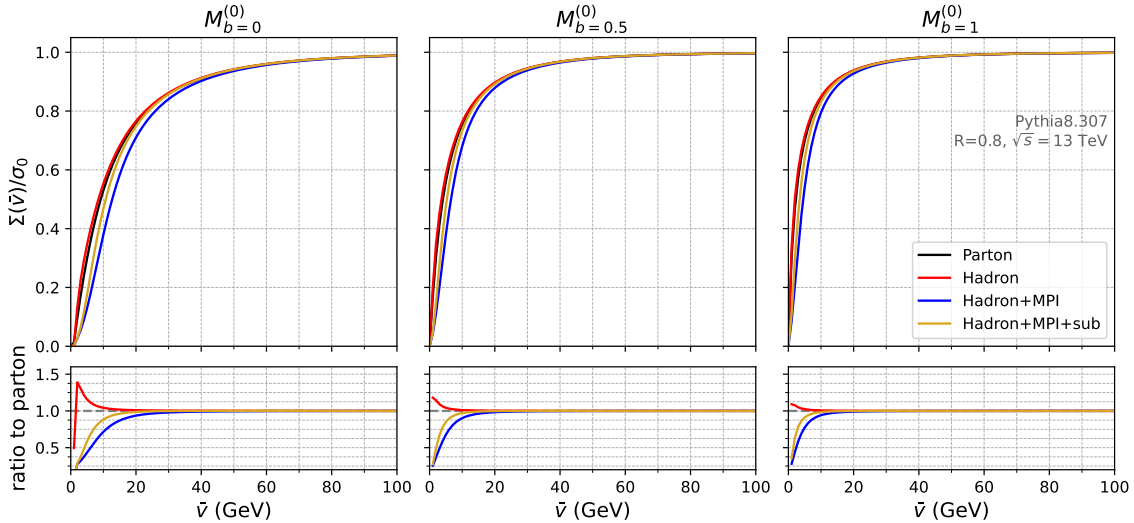


Figure 9: Cumulative distribution for $M_b^{(0)}$ with $b = 0$ (left), $b = 1/2$ (middle) and $b = 1$ (right) as a function of $\bar{v} = v Q$. Shown are four different setups: parton-level (black), hadron-level (red), hadron-level with multi-parton interactions (blue) and hadron-level with multi-parton interactions and area subtraction (yellow). The bottom panel displays the ratio to the parton-level result.

is increased, becoming very small at scales of order $Q M_b^{(0)} \sim 25 - 30$ GeV. This can be compared to the size of the NNLL+NNLO uncertainty band in Fig. 7 which is below 10% at 10 GeV and below 5% at 20 GeV. Moreover, we notice that the impact of the MPI activity depends on the value of b , and it gets reduced for larger b values in line with the fact that radiation at larger absolute rapidities contributes less to the observables. An experimental measurement of these observables for several values of the parameter b could therefore inform about the rapidity distribution of MPIs, which is an aspect that is largely unconstrained so far. To modulate the impact of MPI, one can use the area subtraction algorithm [127, 128] and compute $M_b^{(0)}$ using subtracted jets.¹⁰ After area subtraction, we find less than 10% deviations with respect to parton-level for $Q M_b^{(0)} > 10$ GeV. Therefore, we conclude that $M_b^{(0)}$ is not severely affected by hadronisation and MPI corrections, thus enabling meaningful theory-to-data comparisons.

The results for $S_b^{(0)}$ are shown in Fig. 10. In this case, both hadronisation and MPI corrections are much more sizeable than for $M_b^{(0)}$, in particular when $b \neq 1$. Here, hadronisation corrections lead to a $5 - 10$ GeV shift in the peak of the distribution, while MPI completely distort the shape. This is natural given the fact that the observable does not impose any cut on the jets that enter the sum, see Eq. (2.11), and thus all semi-soft jets arising from MPI have a non-vanishing contribution to $S_b^{(0)}$. This issue affects all additive

¹⁰For LTS involving Lund declusterings, one could also compute the Lund coordinates using subtracted subjets. Alternatives would include, for example, using direct shape subtraction [129], or the `ConstituentSubtractor` method [130] or an event-wide subtraction techniques such as `SoftKiller` [131] or `PUPPI` [132] prior to the clustering.

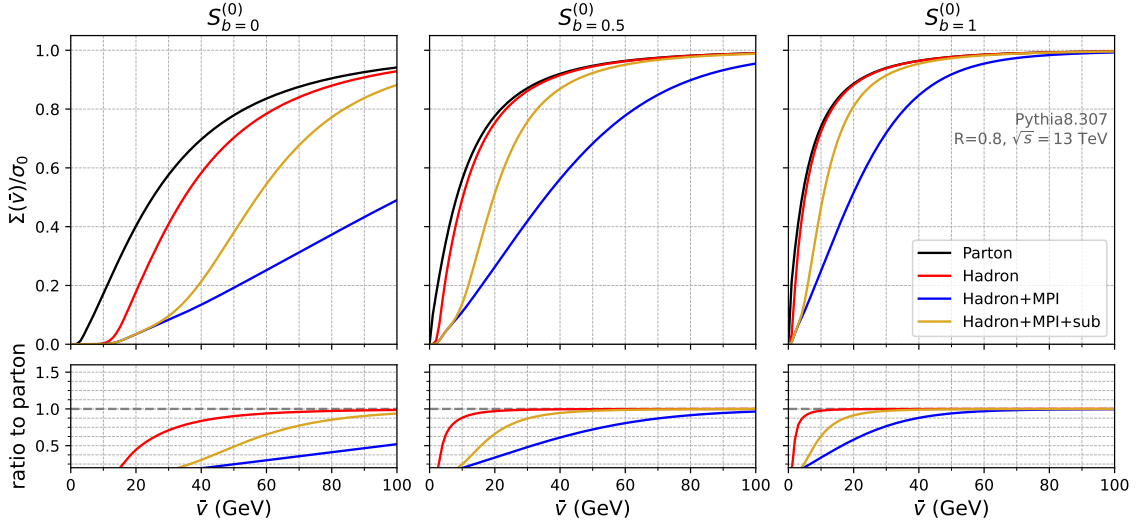


Figure 10: Same as Fig. 9 but for $S_b^{(0)}$.

observables defined without a jet cut. Area subtraction manages to bring the effect of MPI down to a factor of 3, which is still quite large for theory-to-data comparisons. The situation improves slightly when choosing $b = 1$. In this case, hadronisation corrections are of the same size as for $M_{b=1}^{(0)}$, i.e. below 5%, and MPI contamination is also reduced once including area subtraction to less than 10% for $Q S_{b=1}^{(0)} > 40$ GeV. We thus expect large deviations between experimental measurements of $S_b^{(0)}$ and our NNLL+NNLO predictions. To mitigate this discrepancy, one could think about measuring $S_b^{(0)}$ inside groomed jets (cf. Sec. 2.4) instead of at event-wide level. Changing the definition of the observable of course modifies the resummation structure and we thus leave the study of this possibility for future work.

5 Conclusions

In this work, we have introduced Lund-Tree Shapes (LTS), a new class of collider observables defined from the Lund-plane representation of QCD radiation in multi-jet scattering processes. For processes with two emitting legs, these observables were first introduced, at NLL, for the purpose of testing the logarithmic accuracy of parton showers in ee [3], pp [4] and ep [5] collisions. In this article, we presented a generalisation to processes with any number of resolved jets. We also provide a variant of LTS that can be measured on groomed jets, offering an additional tool for the study of jet structure at different collider environments. These observables provide a versatile tool for probing multi-jet final states. At the differential level, LTS behave as continuous, global variables, analogous to classical event shapes and $n \rightarrow n + 1$ jet-resolution parameters, allowing detailed studies of the hierarchical and geometric structure of QCD final states. At the cumulative level, they naturally define jet rates, useful for resolution-based characterisation of multi-jet events or as jet vetoes.

The generality of LTS makes them applicable to scattering processes with any number of resolved jets, across ee , pp and ep colliders, as well as within groomed jets. From a theoretical perspective, they serve as versatile resolution variables for phase-space slicing in higher-order calculations, for matching fixed-order predictions to parton showers, and for testing the logarithmic accuracy of shower algorithms. They also feature good calculability properties, as they are free of non-global logarithmic corrections regardless of the number of jets.

As an initial application, we have presented new NNLL predictions for two-leg processes at ee , pp and ep colliders, and NNLL+NNLO predictions for the LHC, discussing also the practical utility of LTS in collider phenomenology. Beyond these examples, Lund-Tree Shapes offer a promising avenue for systematic studies of multi-jet processes, enabling both precision QCD tests and novel analyses of jet events at present and future collider experiments. The LTS can be easily calculated from the Lund jet plane declusterings obtained from the public version of the `LundPlane` [2] contrib of `FastJet` [133].¹¹

Acknowledgements

We are grateful to Basem El-Menoufi for his contributions in the early stages of this project, and Gavin Salam for discussions and comments on the article. This research was supported by the Italian Ministry of Universities and Research (MUR) under the FIS grant (CUP: D53C24005480001, FLAME) (SFR), the Ramón y Cajal program under grant RYC2022-037846-I and from ERDF (grant PID2024-161668NB-100) (ASO), by the Dutch Research Council (NWO) under project number VI.Veni.232.190 (MvB) and by the European Research Council (ERC) under the European Union’s Horizon 2020 research and innovation programme (grant agreement No. 788223, ASO, GS). The work of LB and PM is funded by the European Union (ERC, grant agreement No. 101044599). Views and opinions expressed are however those of the authors only and do not necessarily reflect those of the European Union or the European Research Council Executive Agency. Neither the European Union nor the granting authority can be held responsible for them.

A Perturbative expansion for resummation ingredients

In this appendix, we will provide the reader with the expressions for the resummation ingredients not provided in the main text, needed to reproduce the results of the paper. Following the main text, we will use the following notation throughout the appendix

$$\alpha_s \equiv \alpha_s(\mu_R), \quad L \equiv \ln \frac{\mu_L}{Qv}, \quad \lambda \equiv \alpha_s \beta_0 L, \quad (\text{A.1})$$

where β_0 is the one-loop QCD β -function, and its value is given in Appendix A.4. The resummation scale μ_L is meant to be replaced with the dynamical definition of Eq. (4.2) in all occurrences.

¹¹Available at <https://fastjet.fr/contrib/>. The implementation of the plugin for DIS is in preparation [134].

A.1 Splitting functions and coefficient functions

The b -dependent coefficient functions $C_{ki}^{(1)}(z)$ are a new result of this work. Before reporting their expression, let us introduce the regularised Altarelli-Parisi splitting functions $\hat{P}_{k,i}(z; \epsilon)$ in $d = 4 - 2\epsilon$ dimensions

$$\begin{aligned}\hat{P}_{qq}(z; \epsilon) &= C_F \left[\frac{1+z^2}{(1-z)_+} - \epsilon(1-z) + \frac{3}{2}\delta(1-z) \right], \\ \hat{P}_{gq}(z; \epsilon) &= C_F \left[\frac{1+(1-z)^2}{z} - \epsilon z \right], \\ \hat{P}_{qg}(z; \epsilon) &= T_R \left[1 - \frac{2z(1-z)}{1-\epsilon} \right] = T_R[1 - 2z(1-z) - 2\epsilon z(1-z)] + \mathcal{O}(\epsilon^2), \\ \hat{P}_{gg}(z; \epsilon) &= \frac{2C_A(1+z^2-z)^2}{z(1-z)_+} + 2\pi\beta_0\delta(1-z).\end{aligned}\tag{A.2}$$

We will denote by $\hat{P}_{ki}^{(0)}(z)$ their expression for $\epsilon \rightarrow 0$, while $\hat{P}_{ki}^{(\epsilon)}(z)$ is the coefficient of the $\mathcal{O}(\epsilon)$ term, i.e.

$$\hat{P}_{ki}(z; \epsilon) = \hat{P}_{ki}^{(0)}(z) + \epsilon \hat{P}_{ki}^{(\epsilon)}(z).\tag{A.3}$$

We also introduce the unregularised splitting function $P_{ki}^{(0)}(z)$, which can be obtained from $\hat{P}_{ki}^{(0)}(z)$ omitting the terms proportional to $\delta(1-z)$ and replacing $(1-z)_+ \rightarrow (1-z)$. In term of these functions, the coefficient functions can be written as

$$\begin{aligned}C_{ki}^{(1)}(z) &= -\hat{P}_{ki}^{(\epsilon)}(z) + \frac{2b}{1+b}(1-z)P_{ki}^{(0)}(z) \left[\left(\frac{\ln(1-z)}{1-z} \right)_+ - \frac{\ln(z)}{1-z} \right] \\ &\quad + 2 \left(\ln \frac{Q}{\mu_F} + \frac{1}{1+b} \ln \frac{\mu_L}{Q} \right) P_{ki}^{(0)}(z).\end{aligned}\tag{A.4}$$

A.2 The Sudakov radiator

The Sudakov radiator \mathcal{R} is separated into a soft (s) and hard-collinear (hc) terms, i.e.

$$\mathcal{R}_{\text{NNLL}}(v) = \sum_{\ell=1}^2 \left[R_s^\ell(v) + R_{\text{hc}}^\ell(v) \right],\tag{A.5}$$

where we also separate contributions associated with radiation from each leg ℓ . At NNLL accuracy, the soft radiator R_s^ℓ reads

$$R_s^\ell(v) = -\frac{\lambda}{\alpha_s \beta_0} g_1^\ell(\lambda) - g_2^\ell(\lambda) - \frac{\alpha_s}{\pi} g_3^\ell(\lambda) - \frac{\alpha_s}{\pi} \delta g_3^\ell(\lambda)\tag{A.6}$$

where

$$\begin{aligned}g_1^\ell(\lambda) &= \frac{C_\ell}{2} \frac{(1+b-2\lambda) \ln \left(1 - \frac{2\lambda}{1+b} \right) - (1-2\lambda) \ln(1-2\lambda)}{\pi b \beta_0}, \\ g_2^\ell(\lambda) &= \frac{C_\ell}{2} \left[\frac{K^{(1)} \left(\ln(1-2\lambda) - (1+b) \ln \left(1 - \frac{2\lambda}{1+b} \right) \right)}{2\pi^2 b \beta_0^2}\right]\end{aligned}\tag{A.7}$$

$$\begin{aligned}
& + \frac{\beta_1(1+b)\ln^2\left(1-\frac{2\lambda}{1+b}\right)}{2\pi b\beta_0^3} + \frac{\beta_1(1+b)\ln\left(1-\frac{2\lambda}{1+b}\right)}{\pi b\beta_0^3} \\
& - \beta_1 \frac{\ln(1-2\lambda)(\ln(1-2\lambda)+2)}{2\pi b\beta_0^3} + \frac{2}{\pi\beta_0} \ln \frac{Q}{\mu_L} \ln\left(1-\frac{2\lambda}{1+b}\right) \\
& + \frac{2}{b\pi\beta_0} \ln \frac{\mu_R}{\mu_L} \left[\ln(1-2\lambda) - (1+b)\ln\left(1-\frac{2\lambda}{1+b}\right) \right] ,
\end{aligned} \tag{A.8}$$

$$\begin{aligned}
g_3^\ell(\lambda) = & \frac{C_\ell}{2} \left[K^{(1)} \frac{\beta_1 \left((1+b+2\lambda)\ln(1-2\lambda) - (1+b)^2(1-2\lambda)\ln\left(1-\frac{2\lambda}{1+b}\right) + 6b\lambda^2 \right)}{2\pi b\beta_0^3(1-2\lambda)(1+b-2\lambda)} \right. \\
& + \frac{\left(\beta_1^2(1+b)^2(1-2\lambda)\ln^2\left(1-\frac{2\lambda}{1+b}\right) - 4b\lambda^2(\beta_0\beta_2 + \beta_1^2) \right)}{2b\beta_0^4(1-2\lambda)(1+b-2\lambda)} \\
& - \frac{\ln(1-2\lambda)(2\beta_0\beta_2(1-2\lambda) + \beta_1^2\ln(1-2\lambda) + 4\beta_1^2\lambda)}{2b\beta_0^4(1-2\lambda)} \\
& + \frac{(1+b)\ln\left(1-\frac{2\lambda}{1+b}\right)(\beta_0\beta_2(1+b-2\lambda) + 2\beta_1^2\lambda)}{b\beta_0^4(1+b-2\lambda)} \\
& - K^{(2)} \frac{\lambda^2}{2\pi^2(1-2\lambda)(1+b-2\lambda)\beta_0^2} \\
& - \ln^2 \frac{\mu_R}{\mu_L} \frac{8\lambda^2}{(1-2\lambda)(1+b-2\lambda)} \\
& + \ln \frac{\mu_R}{\mu_L} \frac{2\beta_1 \left(4b\lambda^2 - (1+b)^2(1-2\lambda)\ln\left(1-\frac{2\lambda}{1+b}\right) + (1+b-2\lambda)\ln(1-2\lambda) \right)}{b\beta_0^2(1-2\lambda)(1+b-2\lambda)} \\
& - \ln \frac{\mu_R}{\mu_L} \frac{4K^{(1)}\lambda^2}{b\beta_0^2(1-2\lambda)(1+b-2\lambda)} \\
& + 4\ln^2 \frac{Q}{\mu_L} \frac{b\lambda}{(1+b)(1+b-2\lambda)} - 4\ln \frac{Q}{\mu_L} \ln \frac{\mu_R}{\mu_L} \cdot \frac{2\lambda}{1+b-2\lambda} \\
& \left. + 4\ln \frac{Q}{\mu_L} \left[\frac{\beta_1}{2\beta_0^2} \frac{2\lambda + (1+b)\cdot\ln(1-\frac{2\lambda}{1+b})}{1+b-2\lambda} - \frac{K^{(1)}\lambda}{2\pi\beta_0(1+b-2\lambda)} \right] \right] ,
\end{aligned} \tag{A.9}$$

$$\delta g_3^\ell(\lambda) = -C_\ell \frac{\pi^2}{6} \frac{\lambda}{(1+b-2\lambda)}. \tag{A.10}$$

The constants $K^{(i)}$ and the QCD beta function coefficients β_i are given in appendix A.4. We also introduce various derivatives of the NLL soft radiator, as they will appear in the evaluation of the transfer function.

$$\mathcal{R}'_{\text{NLL},\ell}(v) \equiv -\frac{\partial [g_1(\alpha_s\beta_0 L)L]}{\partial L} = \frac{C_\ell}{b\pi\beta_0} \left(\ln\left(1-\frac{2\lambda}{1+b}\right) - \ln(1-2\lambda) \right), \tag{A.11a}$$

$$\begin{aligned}
\mathcal{R}'_{\text{NNLL},\ell}(v) \equiv & -\frac{\partial [g_2(\alpha_s\beta_0 L)]}{\partial L} = \frac{C_\ell\alpha_s}{b\pi^2\beta_0^2(1-2\lambda)(1+b-2\lambda)} \left[b\beta_0\lambda K^{(1)} - 2\pi b\beta_1\lambda \right. \\
& \left. - \pi(1+b-2\lambda)\beta_1\ln(1-2\lambda) + \pi(1+b)(1-2\lambda)\beta_1\ln\left(1-\frac{2\lambda}{1+b}\right) \right]
\end{aligned}$$

$$+ \frac{2C_\ell \alpha_s}{\pi} \left[\ln \frac{Q}{\mu_L} (1 - 2\lambda) + \ln \frac{\mu_R}{\mu_L} \frac{2\lambda}{(1 - 2\lambda)(1 + b - 2\lambda)} \right], \quad (\text{A.11b})$$

$$\mathcal{R}_\ell''(v) \equiv \alpha_s \beta_0 \frac{d\mathcal{R}'_{\text{NLL},\ell}}{d\lambda} = 2C_\ell \frac{\alpha_s}{\pi} \frac{1}{(1 - 2\lambda)(1 + b - 2\lambda)}. \quad (\text{A.11c})$$

Notice that by convention the subscript s is dropped. It can be verified that the limit $b \rightarrow 0$ is continuous. We also define the quantities summed over both legs

$$\mathcal{R}'_{\text{NLL}}(v) = \sum_\ell \mathcal{R}'_{\text{NLL},\ell}(v), \quad \mathcal{R}''(v) = \sum_\ell \mathcal{R}''_\ell(v), \quad \mathcal{R}'_{\text{NNLL}}(v) = \sum_\ell \mathcal{R}'_{\text{NNLL},\ell}(v). \quad (\text{A.12})$$

At NNLL accuracy, the hard-collinear radiator reads

$$R_{\text{hc}}(v) = - \sum_\ell \left[h_2^\ell(\lambda) + \frac{\alpha_s}{\pi} h_3^\ell(\lambda) \right], \quad (\text{A.13})$$

with

$$h_2^\ell(\lambda) = \frac{\gamma_\ell^{(0)}}{2\pi\beta_0} \ln \left(1 - \frac{2\lambda}{1+b} \right), \quad (\text{A.14})$$

$$h_3^\ell(\lambda) = \gamma_\ell^{(0)} \frac{\beta_1 \left((1+b) \left(\ln \left(1 - \frac{2\lambda}{1+b} \right) \right) + 2\lambda \right)}{2\beta_0^2 (1+b-2\lambda)} - \gamma_\ell^{(1)} \frac{\lambda}{2\pi\beta_0 (1+b-2\lambda)} + \frac{2\gamma_\ell^{(0)}}{1+b-2\lambda} \left[\frac{b}{1+b} \ln \frac{Q}{\mu_L} - \ln \frac{\mu_R}{\mu_L} \right] \quad (\text{A.15})$$

The constants $\gamma_\ell^{(i)}$ are given in appendix [A.4](#).

A.3 The NNLL transfer function

The transfer function $\mathcal{F}(v)$ is decomposed as

$$\mathcal{F}(v) = \mathcal{F}_{\text{NLL}}(v) + \frac{\alpha_s(\mu_R)}{\pi} \delta\mathcal{F}_{\text{NNLL}}(v). \quad (\text{A.16})$$

The NNLL corrections can be parameterised as follows

$$\delta\mathcal{F}_{\text{NNLL}}(v) = \delta\mathcal{F}_{\text{sc}}(v) + \delta\mathcal{F}_{\text{wa}}(v) + \delta\mathcal{F}_{\text{correl}}(v) + \delta\mathcal{F}_{\text{clust}}(v) + \delta\mathcal{F}_{\text{hc}}(v) + \delta\mathcal{F}_{\text{rec}}(v). \quad (\text{A.17})$$

At NLL we obtain, for ee , pp and ep ,

$$\mathcal{F}_{\text{NLL}}(v) = \begin{cases} 1 & \text{for } M_b^{(n_{\min})}, \\ \frac{e^{-\gamma_E} \mathcal{R}'_{\text{NLL}}(v)}{\Gamma(1 + \mathcal{R}'_{\text{NLL}}(v))} & \text{for } S_b^{(n_{\min})}. \end{cases} \quad (\text{A.18})$$

Below we provide all NNLL corrections.

Soft-collinear correction The soft-collinear correction is 0 for the $M_b^{(n_{\min})}$ observable. For $S_b^{(n_{\min})}$ it reads

$$\begin{aligned}\delta\mathcal{F}_{\text{sc}}(v) = & -\frac{\pi}{\alpha_s}\mathcal{F}_{\text{NLL}}(v)\sum_{\ell=1,2}\left[\mathcal{R}'_{\text{NNLL},\ell}(v)\left(\psi^{(0)}(1+\mathcal{R}'_{\text{NLL}}(v))+\gamma_E\right)\right. \\ & \left.+\frac{\mathcal{R}''_{\ell}(v)}{2}\left(\left(\psi^{(0)}(1+\mathcal{R}'_{\text{NLL}}(v))+\gamma_E\right)^2-\psi^{(1)}(1+\mathcal{R}'_{\text{NLL}}(v))+\frac{\pi^2}{6}\right)\right].\end{aligned}\quad (\text{A.19})$$

where the derivatives of the soft radiator are given in Eqs. A.11. The term in Eq. (A.19) proportional to $\mathcal{R}''_{\ell}(v)$ originates from the expansion of the all-order functional (common in the resummation structure of additive global event shapes)

$$e^{-\frac{\mathcal{R}''}{2}\partial_{\mathcal{R}'}^2}\mathcal{F}_{\text{NLL}}(v), \quad \mathcal{R}''(v) = \sum_{\ell=1,2}\mathcal{R}''_{\ell}, \quad \mathcal{R}'(v) = \sum_{\ell=1,2}\mathcal{R}'_{\ell}, \quad (\text{A.20})$$

that is expanded to second order neglecting N^3LL corrections. In our numerical implementation we leave the above correction unexpanded up to N^3LL corrections, that is we use

$$e^{-\frac{\mathcal{R}''}{2}\partial_{\mathcal{R}'}^2}\mathcal{F}_{\text{NLL}}(v) = e^{-\frac{\mathcal{R}''}{2}\partial_{\mathcal{R}'}^2\ln\mathcal{F}_{\text{NLL}}(v)}\mathcal{F}_{\text{NLL}}(v) + \mathcal{O}(\text{N}^3\text{LL}), \quad (\text{A.21})$$

to prevent the resummed distribution from becoming unphysical (negative) to the left of the Sudakov peak, i.e. at very small values of v , where the $S_b^{(n_{\min})}$ distribution is dominated by non-perturbative corrections.

Wide angle correction The wide-angle correction to the transfer function is zero for the observables we study in this paper in the e^+e^- and ep cases. For pp collisions, the wide-angle correction is zero when considering the observables defined in the partonic c.o.m. frame, while it is given in Eq. (3.29) for the hadronic c.o.m. frame definition. Note that, for ee collisions, the wide-angle correction is the main difference between $M_0^{(2)}$ and the y_{23} Cambridge resolution scale, which is zero for the former but not for the latter.

Correlated correction The correlated correction reads

$$\delta\mathcal{F}_{\text{correl}}(v) = \mathcal{F}_{\text{NLL}}(v)\frac{\lambda\pi\mathcal{R}''(v)}{\alpha_s}(C_A\langle\ln f_{\text{correl}}\rangle_{C_A} + n_f T_R \langle\ln f_{\text{correl}}\rangle_{n_f}). \quad (\text{A.22})$$

We evaluate $\langle\ln f_{\text{correl}}\rangle_{C_A, n_f}$ numerically, and they are defined as

$$\langle\ln f_{\text{correl}}\rangle_{C_A, n_f} = \int_0^\infty \frac{d\zeta}{\zeta} \int_{-\pi}^\pi \frac{d\phi}{2\pi} \int_{-\infty}^\infty d\eta \mathcal{M}_{C_A, n_f} \ln \frac{V_{\text{simple}}^{\text{corr}}(\zeta, \phi, \eta, \beta)}{V_{\text{sc}}(\zeta, \phi, \eta, \beta)} \quad (\text{A.23})$$

where the variables η , ϕ and ζ are given by

$$\eta = \eta_2 - \eta_1, \quad \phi = \phi_2 - \phi_1, \quad \zeta = \frac{k_{t,2}}{k_{t,1}}, \quad (\text{A.24})$$

being $k_{t,i}$, η_i and ϕ_i the transverse momentum, rapidity and azimuth of the soft emission labelled with the index i . The matrix elements are given by

$$\mathcal{M}_{n_f} = \frac{\zeta e^{2\eta} (-\cos(\phi) (\zeta^2 + 2\zeta \cosh(\eta) + 1) + \zeta^2 \cosh(\eta) + 2\zeta + \cosh(\eta))}{2 (\zeta + e^\eta)^2 (\zeta e^\eta + 1)^2 (\cos(\phi) - \cosh(\eta))^2}, \quad (\text{A.25a})$$

$$\begin{aligned} \mathcal{M}_{C_A} = & \frac{-\zeta ((\zeta^2 + 1) \cosh(\eta) \sin^2(\phi) + \zeta \cosh^2(\eta) \cos(2\phi) - \zeta)}{2 (\zeta^2 + 2\zeta \cosh(\eta) + 1)^2 (\cos(\phi) - \cosh(\eta))^2} \\ & - \frac{\cos(\phi)}{2(\cos(\phi) - \cosh(\eta))} - \frac{\sinh^2(\eta) \cos(\phi)}{2 (\zeta^2 + 2\zeta \cosh(\eta) + 1) (\cos(\phi) - \cosh(\eta))^2}. \end{aligned} \quad (\text{A.25b})$$

$V_{\text{simple}}^{\text{corr}}$ is the simple observable for a pair of correlated emissions and is given in terms of the transverse momentum and rapidity of the parent gluon $k = k_1 + k_2$. In the limit $|\eta_1| \gg 1$, we have

$$V_{\text{simple}}^{\text{corr}} = \frac{k_{t,1} e^{-b\eta_1}}{Q} \left(\frac{\zeta + e^\eta}{\zeta e^\eta + 1} \right)^{b/2} e^{-\frac{b\eta}{2}} \sqrt{\zeta^2 + 2\zeta \cos(\phi) + 1}. \quad (\text{A.26})$$

Instead V_{sc} is the value of the observable in the presence of two soft and collinear emissions and it is decomposed into the sum of two pieces

$$V_{\text{sc}}(\zeta, \phi, \eta, b) = V_{\text{clust}}(\zeta, \phi, \eta, b) \Theta_{\text{clust}} + V_{\text{no clust}}(\zeta, \phi, \eta, b) (1 - \Theta_{\text{clust}}), \quad (\text{A.27})$$

where the first term refers to the case in which the two partons cluster together, and the second where they do not. The clustering condition reads

$$\Theta_{\text{clust}} = \begin{cases} \Theta(|\eta| < \ln 2 \cos \phi) \Theta(|\phi| < \pi/3) & \text{for DIS and } ee, \\ \Theta(R^2 - \phi^2 - \eta^2) & \text{for } pp, \end{cases} \quad (\text{A.28})$$

where R is the jet radius. When partons 1 and 2 do not cluster, the observable in the soft collinear limit becomes

$$V_{\text{no clust}}(\zeta, \phi, \eta, b) = \frac{k_{t,1} e^{-b\eta_1}}{Q} \times \begin{cases} 1 + \zeta e^{-b\eta} & \text{for } S_b^{(n_{\min})}, \\ \max(1, \zeta e^{-b\eta}) & \text{for } M_b^{(n_{\min})}, \end{cases} \quad (\text{A.29})$$

and this expression is identical for all processes under consideration. Instead when they cluster

$$V_{\text{clust}}(\zeta, \phi, \eta, b) = \begin{cases} \frac{k_{t,1} e^{-b\eta_1}}{Q} \times \sqrt{\zeta^2 + 2\zeta \cos(\phi) + 1} \left(\frac{(\zeta^2 e^{2\eta} + 2\zeta e^\eta + 1)}{\zeta^2 + 2\zeta \cos(\phi) + 1} \right)^{-\frac{b}{2}} & \text{for DIS and } ee, \\ V_{\text{simple}}^{\text{corr}}(\zeta, \phi, \eta, b) & \text{for } pp. \end{cases} \quad (\text{A.30})$$

The numerical values of $\langle \ln f_{\text{correl}} \rangle C_A$ and $\langle \ln f_{\text{correl}} \rangle_{n_f}$ for DIS and e^+e^- collisions, for $b = 0, 1/2, 1$, are reported in Tab. 1. For the case of $M_0^{(n_{\min})}$, we have verified that our results coincide with those for the Cambridge resolution variable, as presented in Ref. [56].

In Fig. 11, we illustrate the jet-radius (R) dependence of these corrections in pp collisions. Here, one can observe that the correlated correction diverges as $\ln(1/R)$ for $M_b^{(0)}$, as expected. We have also verified that, for small R , our result for $M_0^{(0)}$ agrees numerically with the analytic expansion for the jet veto given in Refs. [9, 135].

Correlated and clustering corrections in DIS and e^+e^- collisions			
Observable	$\langle \ln f_{\text{correl}} \rangle_{C_A}$	$\langle \ln f_{\text{correl}} \rangle_{n_f}$	$\langle \ln f_{\text{clust}} \rangle$
$S_b^{(n_{\min})}$	$b = 0$	0.94426(1)	-0.208545(1)
	$b = 0.5$	0.97044(2)	-0.211395(1)
	$b = 1$	0.94845(3)	-0.238064(2)
$M_b^{(n_{\min})}$	$b = 0$	1.05074(1)	0.014963(3)
	$b = 0.5$	1.08702(2)	0.011683(3)
	$b = 1$	1.09384(3)	-0.018616(2)
$S_b^{(1)}$ and $M_b^{(2)}$			
$S_b^{(1)}$ and $M_b^{(1)}$			

Table 1: Numerical values for $\langle \ln f_{\text{correl}} \rangle_{C_A}$, $\langle \ln f_{\text{correl}} \rangle_{n_f}$, $\langle \ln f_{\text{clust}} \rangle$ for $S_b^{(2)}$ ($S_b^{(1)}$) and $M_b^{(2)}$ ($M_b^{(1)}$) in e^+e^- collisions (DIS) for $b = 0, 1/2, 1$.

Clustering correction The clustering correction is expressed in terms of the same quantities entering the correlated one, and reads

$$\delta \mathcal{F}_{\text{clust}}(v) = \mathcal{F}_{\text{NLL}}(v) \frac{\pi \lambda \mathcal{R}''(v)}{\alpha_s} C_\ell \langle \ln f_{\text{clust}} \rangle, \quad (\text{A.31})$$

with

$$\langle \ln f_{\text{clust}} \rangle = \int_0^\infty \frac{d\zeta}{\zeta} \int_{-\pi}^\pi \frac{d\phi}{2\pi} \int_{-\infty}^\infty d\eta \ln \frac{V_{\text{simple}}^{\text{indip}}(\zeta, \phi, \eta, \beta)}{V_{\text{sc}}(\zeta, \phi, \eta, \beta)} \Theta_{\text{clust}}, \quad (\text{A.32})$$

where $V_{\text{simple}}^{\text{indip}} = V_{\text{no clust}}$ is the simple observable for two independent emissions, and thus always equal to eq. (A.29), while V_{sc} and the clustering condition Θ_{clust} are the same defined in the previous section.

The numerical values of $\langle \ln f_{\text{clust}} \rangle$ for DIS and e^+e^- collisions, for $b = 0, 1/2, 1$, are reported in Tab. 1. For the case of M_0 , we have verified that our results coincide with those for the Cambridge resolution variable, as presented in Ref. [56].

For pp collisions, Eq. (A.32) can be evaluated analytically, yielding for jet radii $R \leq \pi$:

$$\langle \ln f_{\text{clust}}^{pp} \rangle = \begin{cases} \frac{R^4(1+b^2)}{16} & \text{for } S_b^{(0)}, \\ \frac{R^4(1+b^2)}{16} - \frac{\pi^2 R^2}{12} & \text{for } M_b^{(0)}. \end{cases} \quad (\text{A.33})$$

This behaviour is also illustrated in Fig.11. The clustering correction for $M_0^{(0)}$ coincides with the jet veto result presented in Refs. [9, 135].

Recoil correction The recoil correction is present only for final-state legs, and is identical for $S_b^{(n_{\min})}$ and $M_b^{(n_{\min})}$. For ee collisions, we have

$$\begin{aligned} \delta \mathcal{F}_{\text{rec}}^{ee}(v) &= \frac{\mathcal{F}_{\text{NLL}}(v)}{1+b-2\lambda} \\ &\times \begin{cases} C_F \frac{(15-4\pi^2)b - 2(\pi^2-9+9\ln 2)}{6} & \text{for quarks,} \\ C_A \frac{131-132\ln 2-12\pi^2-2(12\pi^2-67)b}{36} + n_f \frac{24\ln 2-23-26b}{36} & \text{for gluons.} \end{cases} \end{aligned} \quad (\text{A.34})$$

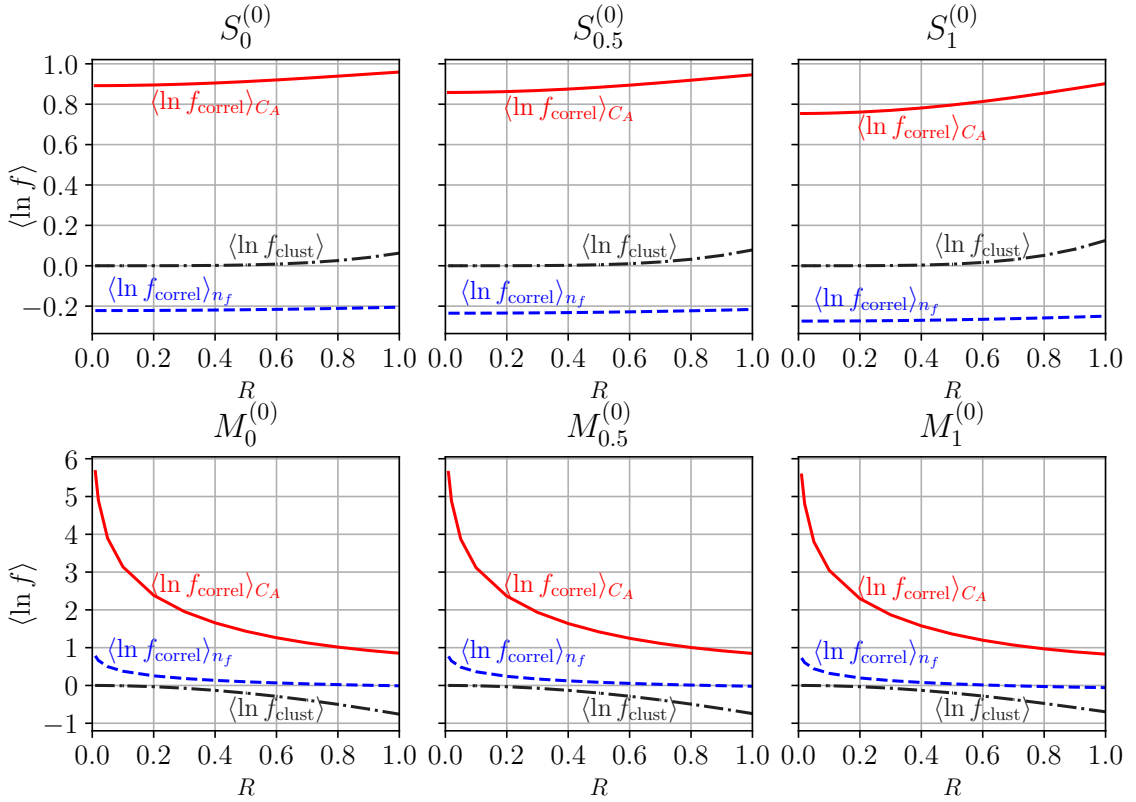


Figure 11: Values for $\langle \ln f_{\text{correl}} \rangle_{CA}$ (red solid line), $\langle \ln f_{\text{correl}} \rangle_{nf}$ (blue dashed line), $\langle \ln f_{\text{clust}} \rangle$ (grey dash-dotted line) for $S_b^{(0)}$ and $M_b^{(0)}$ in pp collision for $b = 0, 1/2, 1$ as a function of the jet radius R for $0 < R \leq 1$.

For ep , since we have only one final-state leg, we have

$$\delta \mathcal{F}_{\text{rec}}^{ep}(v) = \frac{\delta \mathcal{F}_{\text{rec}}^{ee}(v)}{2}. \quad (\text{A.35})$$

Hard-collinear correction The hard collinear correction is 0 for $M_b^{(n_{\min})}$, while for $S_b^{(n_{\min})}$ it reads

$$\delta \mathcal{F}_{\text{hc}}(v) = - \left(\psi^{(0)}(1 + \mathcal{R}'_{\text{NLL}}(v)) + \gamma_E \right) \mathcal{F}_{\text{NLL}}(v) \frac{1}{1+b-2\lambda} \sum_{\ell} \gamma_{\ell}^{(0)}. \quad (\text{A.36})$$

A.4 Constants

The Casimir factor C_{ℓ} for quark and gluon legs reads

$$C_q \equiv C_F = \frac{N_c^2 - 1}{2N_c}, \quad C_g \equiv C_A = N_c, \quad (\text{A.37})$$

with $N_c = 3$. We also consider $n_f = 5$ light quarks. The coefficients of the QCD β function read

$$\beta_0 = \frac{11C_A - 2n_f}{12\pi}, \quad (\text{A.38a})$$

$$\beta_1 = \frac{17C_A^2 - 5C_A n_f - 3C_F n_f}{24\pi^2}, \quad (\text{A.38b})$$

$$\beta_2 = \frac{2857C_A^3 + (54C_F^2 - 615C_F C_A - 1415C_A^2)n_f + (66C_F + 79C_A)n_f^2}{3456\pi^3}. \quad (\text{A.38c})$$

The coefficients of the physical coupling scheme [61, 90, 91] are given by

$$K^{(1)} = C_A \left(\frac{67}{18} - \frac{\pi^2}{6} \right) - \frac{5}{9} n_f, \quad (\text{A.39a})$$

$$\begin{aligned} K^{(2)} = & C_A^2 \left(\frac{245}{24} - \frac{67}{9} \zeta_2 + \frac{11}{6} \zeta_3 + \frac{11}{5} \zeta_2^2 \right) + C_F n_f \left(-\frac{55}{24} + 2\zeta_3 \right) \\ & + C_A n_f \left(-\frac{209}{108} + \frac{10}{9} \zeta_2 - \frac{7}{3} \zeta_3 \right) - \frac{1}{27} n_f^2 + \frac{\pi \beta_0}{2} \left(C_A \left(\frac{808}{27} - 28\zeta_3 \right) - \frac{224}{54} n_f \right). \end{aligned} \quad (\text{A.39b})$$

The hard-collinear anomalous dimensions read

$$\gamma_q^{(0)} = -\frac{3}{2} C_F, \quad \gamma_g^{(0)} = -2\pi\beta_0, \quad (\text{A.40a})$$

$$\gamma_q^{(1)} = -\frac{C_F}{2} \left(C_A \left(\frac{17}{12} + \frac{11\pi^2}{9} - 6\zeta_3 \right) + C_F \left(\frac{3}{4} - \pi^2 + 12\zeta_3 \right) - n_f \left(\frac{1}{6} + \frac{2\pi^2}{9} \right) \right), \quad (\text{A.40b})$$

$$\gamma_g^{(1)} = \frac{n_f}{2} C_F + \frac{2}{3} n_f C_A - C_A^2 \left(\frac{8}{3} + 3\zeta_3 \right). \quad (\text{A.40c})$$

For processes with a final-state quark/gluon leg, the collinear matching coefficients are given by

$$C_{\text{hc},q}^{(1)} = \frac{C_F}{2} \left(1 + \frac{7b}{1+b} \right), \quad (\text{A.41a})$$

$$C_{\text{hc},g}^{(1)} = \left(\frac{b}{1+b} \left(\frac{67}{18} C_A - \frac{13}{9} T_R n_f \right) + \frac{1}{3} T_R n_f \right). \quad (\text{A.41b})$$

Finally we report the hard matching coefficients, including their scale dependence. For e^+e^- and pp we have for the $q\bar{q}$ and gg channels respectively

$$H_q^{(1)} = C_F (\pi^2 - 8) - \frac{4C_F}{1+b} \ln^2 \frac{Q}{\mu_L} - 4 \frac{\gamma_q^{(0)}}{1+b} \ln \frac{Q}{\mu_L}, \quad (\text{A.42})$$

$$H_g^{(1)} = C_A (\pi^2 + 5) - 3C_F - \frac{4C_A}{1+b} \ln^2 \frac{Q}{\mu_L} - 4 \frac{\gamma_g^{(0)}}{1+b} \ln \frac{Q}{\mu_L} + 8\pi\beta_0 \ln \frac{\mu_R}{Q}. \quad (\text{A.43})$$

For DIS, the constants can be obtained via crossing and read

$$H_{q,g}^{(1),\text{DIS}} = H_{q,g}^{(1)} - C_{F,A} \pi^2. \quad (\text{A.44})$$

B A prescription for switching off logarithms in matching

In this section we provide additional details on the matching prescription introduced in Sec. 4.1. The dynamical resummation scale given in Eqs. (4.2), (4.3) is characterised by three regions: a *resummation* region ($v < v_M$), a *matching* region ($v_M \leq v < 1$), and a *fixed-order* region ($v \geq 1$). Such a simple prescription guarantees that the dependence of the prediction on the resummation scale μ_L is confined at small v , where its variation probes higher-order logarithmic corrections, while the matching scale μ_M determines the scale at which the matched prediction reduces to its fixed-order component.

The function $\mathfrak{r}(v)$ is given by the polynomial $\mathfrak{r}(v) = r_0 + \sum_{i=0}^n r_{i+1} v^{p+i}$, where p is a positive power chosen such that we introduce at most quadratic power corrections at small v ($p \geq 2$). The coefficients are determined by imposing the following matching conditions

$$\mathfrak{r}(0) = r_0 = \mu_L, \quad \mathfrak{r}(v_M) = \mu_M, \quad \left. \frac{d^k}{dv^k} \ln \frac{\mathfrak{r}(v)}{v} \right|_{v=v_M} = 0 \quad \text{for } k = 1, \dots, n, \quad (\text{B.1})$$

and solving the corresponding linear system. For $n = 2$, we obtain

$$\begin{aligned} r_0 &= \mu_L, & r_1 &= \frac{1}{2} (1+p) v_M^{-p} (p v_M Q - (2+p) \mu_L), \\ r_2 &= v_M^{-1-p} ((1-p^2) v_M Q + p(2+p) \mu_L), & r_3 &= -\frac{1}{2} p v_M^{-2-p} ((1-p) v_M Q + (1+p) \mu_L). \end{aligned} \quad (\text{B.2})$$

Similarly, the function $\mathfrak{m}(v)$ is given by an analogous polynomial $\mathfrak{m}(v) = m_0 + \sum_{i=0}^{2s} m_{i+1} v^{q+i}$ (where q is a positive parameter, in general different from p), satisfying the constraints

$$\mathfrak{m}\left(\frac{\mu_M}{Q}\right) = \mu_M, \quad \mathfrak{m}(1) = Q, \quad \left. \frac{d^k}{dv^k} \ln \frac{\mathfrak{m}(v)}{v} \right|_{v=v_M} = \left. \frac{d^k}{dv^k} \ln \frac{\mathfrak{m}(v)}{v} \right|_{v=1} = 0 \quad \text{for } k = 1, \dots, s. \quad (\text{B.3})$$

For $s = 1$ we obtain

$$m_0 = \frac{Q v_M \left(-((v_M + 1) v_M^q) - q(1 - v_M) (v_M^q + 1) + v_M + 1 \right)}{2 v_M (1 - v_M^q) - q(1 - v_M) (v_M^{q+1} + 1)}, \quad (\text{B.4a})$$

$$m_1 = -\frac{Q v_M \left(v_M^{-q} + v_M^{q+2} - (q+1)^2 v_M^2 + 2q(q+2) v_M - (q+1)^2 \right)}{(1 - v_M) \left(2 v_M (1 - v_M^q) - q(1 - v_M) (v_M^{q+1} + 1) \right)}, \quad (\text{B.4b})$$

$$m_2 = -\frac{Q v_M^{-q} \left(-2 v_M^{2q+2} + (v_M + 1) (q(q+1)(1 - v_M)^2 + 2 v_M) v_M^q - 2 v_M \right)}{(1 - v_M) \left(2 v_M (1 - v_M^q) - q(1 - v_M) (v_M^{q+1} + 1) \right)}, \quad (\text{B.4c})$$

$$m_3 = -\frac{Q v_M^{-q} \left(-((q^2(1 - v_M)^2 + 2 v_M) v_M^q) + v_M^{2q+1} + v_M \right)}{(1 - v_M) \left(2 v_M (1 - v_M^q) - q(1 - v_M) (v_M^{q+1} + 1) \right)}. \quad (\text{B.4d})$$

One can verify that the limit $v_M \rightarrow 1$ is smooth. With reference to Eq. (4.1), both L and $\ln \frac{Q}{\mu_L}$ are active in the resummation region, while only the latter remains in the

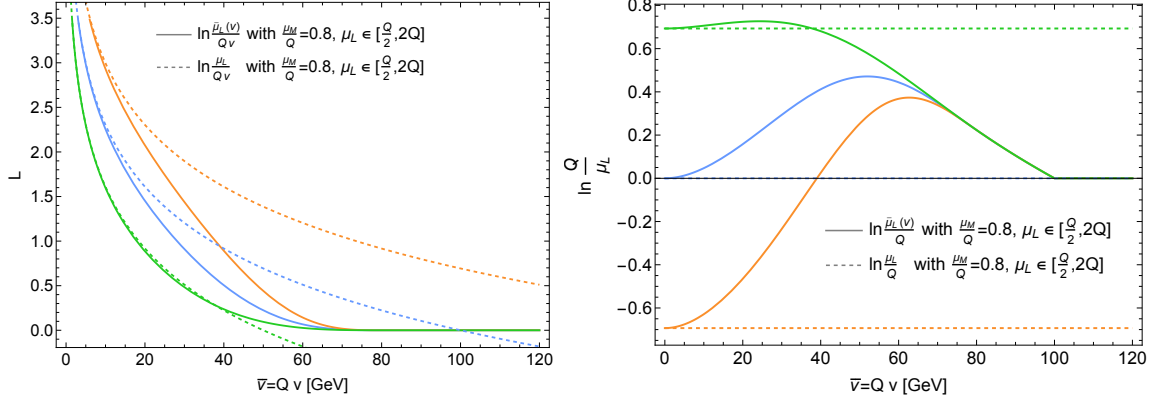


Figure 12: Comparison between logarithms with the dynamical and fixed resummation scales, for a variation of the scale μ_L in Eq. (4.2). The left plot shows the behaviour of the resummed logarithm L in Eq. (4.1), while the right plot shows the term $\ln Q/\mu_L$ in the same equation. In all cases the hard scale is set to $Q = 100$ GeV.

matching region where no large logarithms are present. To help visualise the action of the dynamical scales, in Fig. 12 we show an example obtained with $p = q = 2$, $Q = 100$ GeV and $\mu_M = 80$ GeV. We clearly see that both L and $\ln Q/\mu_L$ are affected by the prescription in the resummation region, ensuring that at small $\bar{v} = Qv$ they agree with their unmodified counterparts. At $\bar{v} = \mu_M$, the resummed logarithm L is turned off according to the function $\mathbf{r}(v)$, while only $\ln Q/\mu_L$ is nonzero in the matching region $\mu_M \leq \bar{v} < Q$, where it is eventually turned off at $\bar{v} = Q$ following the function $\mathbf{m}(v)$. It is important to stress that the dependence of $\mathbf{m}(v)$ completely cancels out at the level of the matched prediction (4.6), so that a variation of μ_M only determines the scale at which the fixed-order result is recovered. Finally, the fixed-order region is not affected by any of the above scales. Together with variations of the factorisation and renormalisation scales, this provides a flexible way to access perturbative uncertainties in applications to phenomenology.

C Fixed-order validation up to second perturbative order for ep and ee

This appendix contains the validation of the resummation for the LTS for ep and ee up to second perturbative order. The corresponding pp validations were discussed in Sec 3.4. We start by discussing the results for ep . The fixed-order reference results are obtained with `disorder` [116–118] (with `cutoff` = 10^{-14} and `npow1` = 6 and `npow2` = 4). We perform the check at a fixed Born point given by $x_{\text{DIS}} = 0.3$ and $Q = 91.1876$ GeV. We use central values for the renormalisation and factorisation scales, and employ the central replica of the `NNPDF40MC_nnlo_as_01180` PDF set. We then compute the quantity $\Delta f(v)$ (see Eq. (3.51)) at NLO and NNLO for $S_b^{(1)}$ and $M_b^{(1)}$. The results are shown in Fig. 13. In the top panel we show the NLO comparison, and in the bottom two panels the NNLO one. We observe the expected convergence for $v \rightarrow 0$. In Fig. 14 we also show the convergence of the difference between the $M_b^{(0)}$ and $S_b^{(0)}$ observables, which tends to behave better due

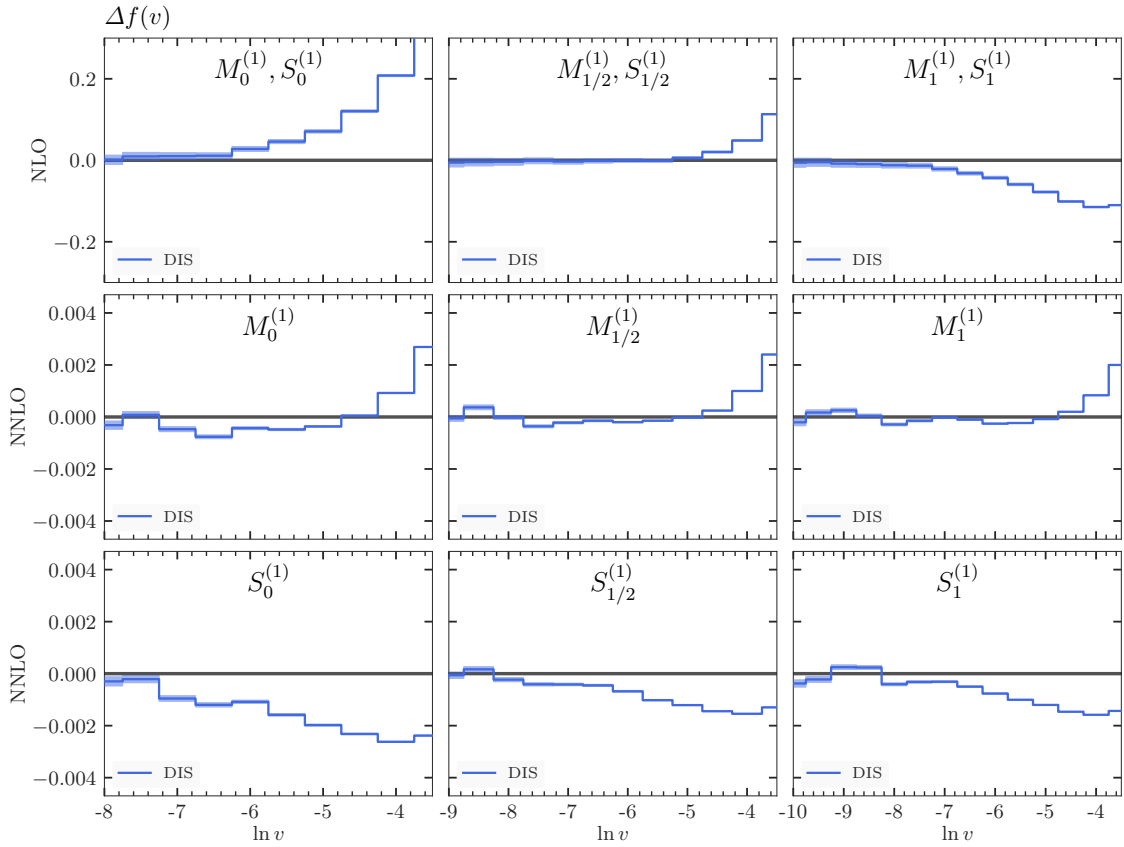


Figure 13: Difference between the fixed-order and resummed-expanded differential cross sections, normalised to the Born cross section, c.f. Eq. (3.51), for DIS. We consider three values of b , $b = 0$ (left), $b = 1/2$ (middle) $b = 1$ (right). The top panel shows the NLO comparison for $S_b^{(1)}/M_b^{(1)}$. The middle (bottom) panel shows the NNLO comparison for $M_b^{(1)}$ ($S_b^{(1)}$). The bands show the statistical uncertainty.

to cancellations of the larger logarithmic powers as well as statistical uncertainties in this quantity. This gives us further confidence that our prediction is correct.

We now move to the ee validation. We ran `Event2` [116] in quadruple precision (with `cutoff` = 10^{-16} and `npow1` = `npow2` = 6) and compared the resulting predictions with the fixed-order expansion of our resummation prediction. The result can be found in Fig. 15, displaying a successful test for all LTS.

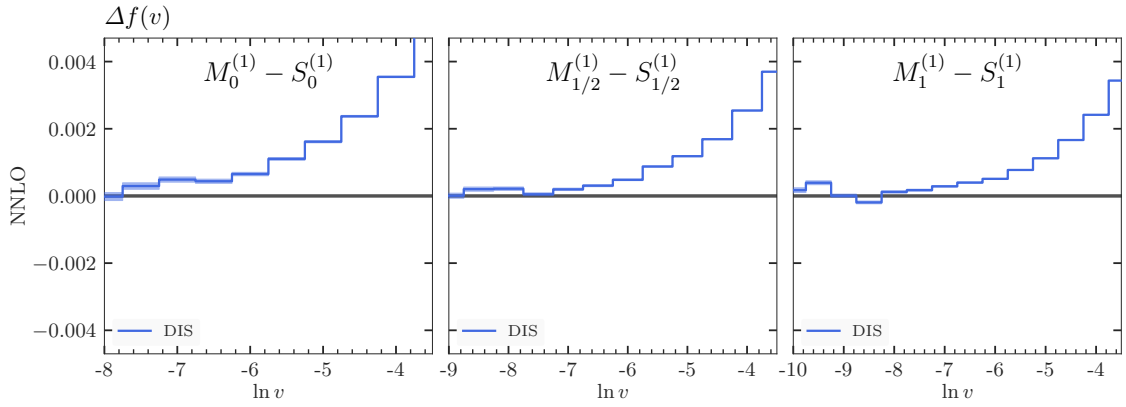


Figure 14: Same as Fig. 13, but for the difference between the $M_b^{(1)}$ and $S_b^{(1)}$ observables.

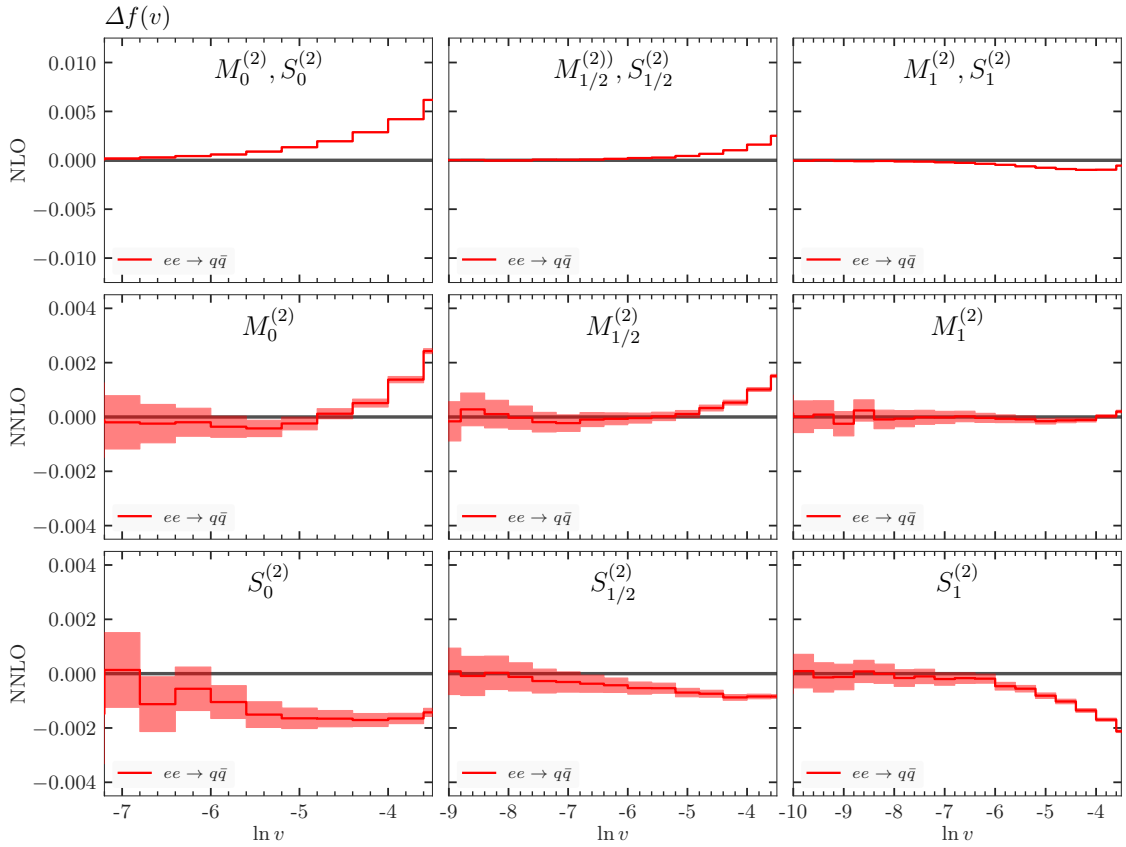


Figure 15: Same as Fig. 13, but for e^+e^- .

References

- [1] B. Andersson, G. Gustafson, L. Lonnblad and U. Pettersson, *Coherence Effects in Deep Inelastic Scattering*, *Z. Phys. C* **43** (1989) 625.
- [2] F. A. Dreyer, G. P. Salam and G. Soyez, *The Lund Jet Plane*, *JHEP* **12** (2018) 064,

[1807.04758].

- [3] M. Dasgupta, F. A. Dreyer, K. Hamilton, P. F. Monni, G. P. Salam and G. Soyez, *Parton showers beyond leading logarithmic accuracy*, *Phys. Rev. Lett.* **125** (2020) 052002, [2002.11114].
- [4] M. van Beekveld, S. Ferrario Ravasio, K. Hamilton, G. P. Salam, A. Soto-Ontoso, G. Soyez et al., *PanScales showers for hadron collisions: all-order validation*, *JHEP* **11** (2022) 020, [2207.09467].
- [5] M. van Beekveld and S. Ferrario Ravasio, *Next-to-leading-logarithmic PanScales showers for Deep Inelastic Scattering and Vector Boson Fusion*, *JHEP* **02** (2024) 001, [2305.08645].
- [6] M. Dasgupta and G. P. Salam, *Event shapes in $e^+ e^-$ annihilation and deep inelastic scattering*, *J. Phys. G* **30** (2004) R143, [hep-ph/0312283].
- [7] A. Banfi, G. P. Salam and G. Zanderighi, *Phenomenology of event shapes at hadron colliders*, *JHEP* **06** (2010) 038, [1001.4082].
- [8] G. Stagnitto, *Jets at electron-positron colliders*, 8, 2025. 2508.14700.
- [9] A. Banfi, P. F. Monni, G. P. Salam and G. Zanderighi, *Higgs and Z-boson production with a jet veto*, *Phys. Rev. Lett.* **109** (2012) 202001, [1206.4998].
- [10] T. Becher, M. Neubert and L. Rothen, *Factorization and $N^3LL_p + NNLO$ predictions for the Higgs cross section with a jet veto*, *JHEP* **10** (2013) 125, [1307.0025].
- [11] I. W. Stewart, F. J. Tackmann, J. R. Walsh and S. Zuberi, *Jet p_T resummation in Higgs production at $NNLL' + NNLO$* , *Phys. Rev. D* **89** (2014) 054001, [1307.1808].
- [12] T. Becher, R. Frederix, M. Neubert and L. Rothen, *Automated $NNLL + NLO$ resummation for jet-veto cross sections*, *Eur. Phys. J. C* **75** (2015) 154, [1412.8408].
- [13] A. Banfi, F. Caola, F. A. Dreyer, P. F. Monni, G. P. Salam, G. Zanderighi et al., *Jet-vetoed Higgs cross section in gluon fusion at $N^3LO + NNLL$ with small- R resummation*, *JHEP* **04** (2016) 049, [1511.02886].
- [14] S. Gangal, M. Stahlhofen and F. J. Tackmann, *Rapidity-Dependent Jet Veto*, *Phys. Rev. D* **91** (2015) 054023, [1412.4792].
- [15] P. F. Monni, L. Rottoli and P. Torrielli, *Higgs transverse momentum with a jet veto: a double-differential resummation*, *Phys. Rev. Lett.* **124** (2020) 252001, [1909.04704].
- [16] S. Gangal, J. R. Gaunt, F. J. Tackmann and E. Vryonidou, *Higgs Production at $NNLL' + NNLO$ using Rapidity Dependent Jet Veto*, *JHEP* **05** (2020) 054, [2003.04323].
- [17] T. Clark, S. Gangal and J. R. Gaunt, *The Drell-Yan process at $NNLL' + NNLO$ using rapidity dependent jet vetoes*, *JHEP* **08** (2025) 060, [2504.06353].
- [18] S. Catani and M. Grazzini, *An NNLO subtraction formalism in hadron collisions and its application to Higgs boson production at the LHC*, *Phys. Rev. Lett.* **98** (2007) 222002, [hep-ph/0703012].
- [19] J. Gaunt, M. Stahlhofen, F. J. Tackmann and J. R. Walsh, *N -jettiness Subtractions for NNLO QCD Calculations*, *JHEP* **09** (2015) 058, [1505.04794].
- [20] R. Boughezal, C. Focke, X. Liu and F. Petriello, *W -boson production in association with a jet at next-to-next-to-leading order in perturbative QCD*, *Phys. Rev. Lett.* **115** (2015) 062002, [1504.02131].

[21] L. Buonocore, M. Grazzini, J. Haag, L. Rottoli and C. Savoini, *Effective transverse momentum in multiple jet production at hadron colliders*, *Phys. Rev. D* **106** (2022) 014008, [[2201.11519](#)].

[22] S. Abreu, J. R. Gaunt, P. F. Monni, L. Rottoli and R. Szafron, *Quark and gluon two-loop beam functions for leading-jet p_T and slicing at NNLO*, *JHEP* **04** (2023) 127, [[2207.07037](#)].

[23] L. Buonocore, M. Grazzini, J. Haag, L. Rottoli and C. Savoini, *Exploring slicing variables for jet processes*, *JHEP* **12** (2023) 193, [[2307.11570](#)].

[24] R.-J. Fu, R. Rahn, D. Y. Shao, W. J. Waalewijn and B. Wu, *qT Slicing with Multiple Jets*, *Phys. Rev. Lett.* **135** (2025) 171903, [[2412.05358](#)].

[25] K. Hamilton, P. Nason, C. Oleari and G. Zanderighi, *Merging $H/W/Z + 0$ and 1 jet at NLO with no merging scale: a path to parton shower + NNLO matching*, *JHEP* **05** (2013) 082, [[1212.4504](#)].

[26] K. Hamilton, P. Nason, E. Re and G. Zanderighi, *NNLOPS simulation of Higgs boson production*, *JHEP* **10** (2013) 222, [[1309.0017](#)].

[27] S. Alioli, C. W. Bauer, C. Berggren, F. J. Tackmann, J. R. Walsh and S. Zuberi, *Matching Fully Differential NNLO Calculations and Parton Showers*, *JHEP* **06** (2014) 089, [[1311.0286](#)].

[28] S. Alioli, C. W. Bauer, C. Berggren, F. J. Tackmann and J. R. Walsh, *Drell-Yan production at NNLL'+NNLO matched to parton showers*, *Phys. Rev. D* **92** (2015) 094020, [[1508.01475](#)].

[29] S. Alioli, C. W. Bauer, A. Broggio, A. Gavardi, S. Kallweit, M. A. Lim et al., *Matching NNLO predictions to parton showers using N3LL color-singlet transverse momentum resummation in geneva*, *Phys. Rev. D* **104** (2021) 094020, [[2102.08390](#)].

[30] P. F. Monni, P. Nason, E. Re, M. Wiesemann and G. Zanderighi, *MiNNLOPS: a new method to match NNLO QCD to parton showers*, *JHEP* **05** (2020) 143, [[1908.06987](#)].

[31] P. F. Monni, E. Re and M. Wiesemann, *MiNNLOPS: optimizing $2 \rightarrow 1$ hadronic processes*, *Eur. Phys. J. C* **80** (2020) 1075, [[2006.04133](#)].

[32] J. Mazzitelli, P. F. Monni, P. Nason, E. Re, M. Wiesemann and G. Zanderighi, *Next-to-Next-to-Leading Order Event Generation for Top-Quark Pair Production*, *Phys. Rev. Lett.* **127** (2021) 062001, [[2012.14267](#)].

[33] A. Gavardi, M. A. Lim, S. Alioli and F. J. Tackmann, *NNLO+PS $W^+ W^-$ production using jet veto resummation at NNLL'*, *JHEP* **12** (2023) 069, [[2308.11577](#)].

[34] M. van Beekveld, S. Ferrario Ravasio, J. Helliwell, A. Karlberg, G. P. Salam, L. Scyboz et al., *Logarithmically-accurate and positive-definite NLO shower matching*, *JHEP* **10** (2025) 038, [[2504.05377](#)].

[35] M. Dasgupta, F. A. Dreyer, K. Hamilton, P. F. Monni and G. P. Salam, *Logarithmic accuracy of parton showers: a fixed-order study*, *JHEP* **09** (2018) 033, [[1805.09327](#)].

[36] K. Hamilton, R. Medves, G. P. Salam, L. Scyboz and G. Soyez, *Colour and logarithmic accuracy in final-state parton showers*, *JHEP* **03** (2021) 041, [[2011.10054](#)].

[37] A. Karlberg, G. P. Salam, L. Scyboz and R. Verheyen, *Spin correlations in final-state parton showers and jet observables*, *Eur. Phys. J. C* **81** (2021) 681, [[2103.16526](#)].

[38] K. Hamilton, A. Karlberg, G. P. Salam, L. Scyboz and R. Verheyen, *Soft spin correlations in final-state parton showers*, *JHEP* **03** (2022) 193, [[2111.01161](#)].

[39] M. van Beekveld, S. Ferrario Ravasio, G. P. Salam, A. Soto-Ontoso, G. Soyez and R. Verheyen, *PanScales parton showers for hadron collisions: formulation and fixed-order studies*, *JHEP* **11** (2022) 019, [[2205.02237](#)].

[40] J. R. Forshaw, J. Holguin and S. Plätzer, *Building a consistent parton shower*, *JHEP* **09** (2020) 014, [[2003.06400](#)].

[41] Z. Nagy and D. E. Soper, *Summations by parton showers of large logarithms in electron-positron annihilation*, [2011.04777](#).

[42] Z. Nagy and D. E. Soper, *Summations of large logarithms by parton showers*, *Phys. Rev. D* **104** (2021) 054049, [[2011.04773](#)].

[43] F. Herren, S. Höche, F. Krauss, D. Reichelt and M. Schoenherr, *A new approach to color-coherent parton evolution*, *JHEP* **10** (2023) 091, [[2208.06057](#)].

[44] B. Assi and S. Höche, *New approach to QCD final-state evolution in processes with massive partons*, *Phys. Rev. D* **109** (2024) 114008, [[2307.00728](#)].

[45] C. T. Preuss, *A partitioned dipole-antenna shower with improved transverse recoil*, *JHEP* **07** (2024) 161, [[2403.19452](#)].

[46] S. Höche, F. Krauss and D. Reichelt, *The Alaric parton shower for hadron colliders*, [2404.14360](#).

[47] M. van Beekveld, M. Dasgupta, B. K. El-Menoufi, J. Helliwell, P. F. Monni and G. P. Salam, *A collinear shower algorithm for NSL non-singlet fragmentation*, *JHEP* **03** (2025) 209, [[2409.08316](#)].

[48] M. van Beekveld et al., *New Standard for the Logarithmic Accuracy of Parton Showers*, *Phys. Rev. Lett.* **134** (2025) 011901, [[2406.02661](#)].

[49] S. Höche, F. Krauss, P. Meinzinger and D. Reichelt, *Recoil-Safe Subtraction, Matching and Merging in $e^+e^- \rightarrow \text{hadrons}$* , [2507.22837](#).

[50] Y. L. Dokshitzer, G. D. Leder, S. Moretti and B. R. Webber, *Better jet clustering algorithms*, *JHEP* **08** (1997) 001, [[hep-ph/9707323](#)].

[51] M. Wobisch and T. Wengler, *Hadronization corrections to jet cross-sections in deep inelastic scattering*, in *Workshop on Monte Carlo Generators for HERA Physics (Plenary Starting Meeting)*, pp. 270–279, 4, 1998. [hep-ph/9907280](#).

[52] D. Bertolini, T. Chan and J. Thaler, *Jet Observables Without Jet Algorithms*, *JHEP* **04** (2014) 013, [[1310.7584](#)].

[53] A. J. Larkoski, D. Neill and J. Thaler, *Jet Shapes with the Broadening Axis*, *JHEP* **04** (2014) 017, [[1401.2158](#)].

[54] S. Alioli, P. Nason, C. Oleari and E. Re, *A general framework for implementing NLO calculations in shower Monte Carlo programs: the POWHEG BOX*, *JHEP* **06** (2010) 043, [[1002.2581](#)].

[55] A. Banfi, G. P. Salam and G. Zanderighi, *Semi-numerical resummation of event shapes*, *JHEP* **01** (2002) 018, [[hep-ph/0112156](#)].

[56] A. Banfi, H. McAslan, P. F. Monni and G. Zanderighi, *The two-jet rate in e^+e^- at next-to-next-to-leading-logarithmic order*, *Phys. Rev. Lett.* **117** (2016) 172001, [[1607.03111](#)].

[57] S. Brandt, C. Peyrou, R. Sosnowski and A. Wroblewski, *The Principal axis of jets. An Attempt to analyze high-energy collisions as two-body processes*, *Phys. Lett.* **12** (1964) 57–61.

[58] E. Farhi, *A QCD Test for Jets*, *Phys. Rev. Lett.* **39** (1977) 1587–1588.

[59] T. Becher and M. D. Schwartz, *A precise determination of α_s from LEP thrust data using effective field theory*, *JHEP* **07** (2008) 034, [[0803.0342](#)].

[60] A. Banfi, G. P. Salam and G. Zanderighi, *Principles of general final-state resummation and automated implementation*, *JHEP* **03** (2005) 073, [[hep-ph/0407286](#)].

[61] A. Banfi, B. K. El-Menoufi and P. F. Monni, *The Sudakov radiator for jet observables and the soft physical coupling*, *JHEP* **01** (2019) 083, [[1807.11487](#)].

[62] C. F. Berger, T. Kucs and G. F. Sterman, *Event shape / energy flow correlations*, *Phys. Rev. D* **68** (2003) 014012, [[hep-ph/0303051](#)].

[63] G. Bell, A. Hornig, C. Lee and J. Talbert, *e^+e^- angularity distributions at NNLL' accuracy*, *JHEP* **01** (2019) 147, [[1808.07867](#)].

[64] I. W. Stewart, F. J. Tackmann and W. J. Waalewijn, *N -Jettiness: An Inclusive Event Shape to Veto Jets*, *Phys. Rev. Lett.* **105** (2010) 092002, [[1004.2489](#)].

[65] F. Halzen, A. D. Martin, D. M. Scott and M. P. Tuite, *The Transverse Hadronic Energy Accompanying Weak Bosons*, *Z. Phys. C* **14** (1982) 351.

[66] C. T. H. Davies and B. R. Webber, *Transverse Hadronic Energy Emission in Hard Scattering Processes*, *Z. Phys. C* **24** (1984) 133.

[67] G. Altarelli, G. Martinelli and F. Rapuano, *The Transverse Hadronic Energy in W and Z^0 Production*, *Z. Phys. C* **32** (1986) 369–375.

[68] A. Papaefstathiou, J. M. Smillie and B. R. Webber, *Resummation of transverse energy in vector boson and Higgs boson production at hadron colliders*, *JHEP* **04** (2010) 084, [[1002.4375](#)].

[69] M. Grazzini, A. Papaefstathiou, J. M. Smillie and B. R. Webber, *Resummation of the transverse-energy distribution in Higgs boson production at the Large Hadron Collider*, *JHEP* **09** (2014) 056, [[1403.3394](#)].

[70] B. R. Webber, *Factorization and jet clustering algorithms for deep inelastic scattering*, *J. Phys. G* **19** (1993) 1567–1575.

[71] V. Antonelli, M. Dasgupta and G. P. Salam, *Resummation of thrust distributions in DIS*, *JHEP* **02** (2000) 001, [[hep-ph/9912488](#)].

[72] D. Kang, C. Lee and I. W. Stewart, *Using 1-Jettiness to Measure 2 Jets in DIS 3 Ways*, *Phys. Rev. D* **88** (2013) 054004, [[1303.6952](#)].

[73] Z.-B. Kang, S. Mantry and J.-W. Qiu, *N -Jettiness as a Probe of Nuclear Dynamics*, *Phys. Rev. D* **86** (2012) 114011, [[1204.5469](#)].

[74] J.-H. Ee, D. Kang, C. Lee and I. W. Stewart, *Precision DIS thrust predictions for HERA and EIC*, *JHEP* **07** (2025) 240, [[2504.05234](#)].

[75] H. Cao, Z.-B. Kang, X. Liu and S. Mantry, *One-jettiness DIS event shape at N3LL+ $O(\alpha s^2)$* , *Phys. Rev. D* **110** (2024) 014045, [[2401.01941](#)].

[76] A. J. Larkoski, S. Marzani, G. Soyez and J. Thaler, *Soft Drop*, *JHEP* **05** (2014) 146, [[1402.2657](#)].

[77] M. Dasgupta, A. Fregoso, S. Marzani and G. P. Salam, *Towards an understanding of jet substructure*, *JHEP* **09** (2013) 029, [[1307.0007](#)].

[78] C. Frye, A. J. Larkoski, M. D. Schwartz and K. Yan, *Factorization for groomed jet substructure beyond the next-to-leading logarithm*, *JHEP* **07** (2016) 064, [[1603.09338](#)].

[79] S. Marzani, L. Schunk and G. Soyez, *The jet mass distribution after Soft Drop*, *Eur. Phys. J. C* **78** (2018) 96, [[1712.05105](#)].

[80] S. Marzani, L. Schunk and G. Soyez, *A study of jet mass distributions with grooming*, *JHEP* **07** (2017) 132, [[1704.02210](#)].

[81] Z.-B. Kang, K. Lee, X. Liu and F. Ringer, *Soft drop groomed jet angularities at the LHC*, *Phys. Lett. B* **793** (2019) 41–47, [[1811.06983](#)].

[82] A. Kardos, A. J. Larkoski and Z. Trócsányi, *Groomed jet mass at high precision*, *Phys. Lett. B* **809** (2020) 135704, [[2002.00942](#)].

[83] D. Anderle, M. Dasgupta, B. K. El-Menoufi, J. Helliwell and M. Guzzi, *Groomed jet mass as a direct probe of collinear parton dynamics*, *Eur. Phys. J. C* **80** (2020) 827, [[2007.10355](#)].

[84] M. Dasgupta and B. K. El-Menoufi, *Dissecting the collinear structure of quark splitting at NNLL*, *JHEP* **12** (2021) 158, [[2109.07496](#)].

[85] M. Dasgupta, B. K. El-Menoufi and J. Helliwell, *QCD resummation for groomed jet observables at NNLL+NLO*, *JHEP* **01** (2023) 045, [[2211.03820](#)].

[86] M. van Beekveld, M. Dasgupta, B. K. El-Menoufi, J. Helliwell and P. F. Monni, *Collinear fragmentation at NNLL: generating functionals, groomed correlators and angularities*, *JHEP* **05** (2024) 093, [[2307.15734](#)].

[87] F. A. Dreyer, L. Necib, G. Soyez and J. Thaler, *Recursive Soft Drop*, *JHEP* **06** (2018) 093, [[1804.03657](#)].

[88] A. Banfi, H. McAslan, P. F. Monni and G. Zanderighi, *A general method for the resummation of event-shape distributions in e^+e^- annihilation*, *JHEP* **05** (2015) 102, [[1412.2126](#)].

[89] L. Arpino, A. Banfi and B. K. El-Menoufi, *Near-to-planar three-jet events at NNLL accuracy*, *JHEP* **07** (2020) 171, [[1912.09341](#)].

[90] S. Catani, B. R. Webber and G. Marchesini, *QCD coherent branching and semiinclusive processes at large x* , *Nucl. Phys. B* **349** (1991) 635–654.

[91] S. Catani, D. De Florian and M. Grazzini, *Soft-gluon effective coupling and cusp anomalous dimension*, *Eur. Phys. J. C* **79** (2019) 685, [[1904.10365](#)].

[92] W. Bizon, P. F. Monni, E. Re, L. Rottoli and P. Torrielli, *Momentum-space resummation for transverse observables and the Higgs p_\perp at $N^3LL+NNLO$* , *JHEP* **02** (2018) 108, [[1705.09127](#)].

[93] M. Dasgupta and G. P. Salam, *Resummation of nonglobal QCD observables*, *Phys. Lett. B* **512** (2001) 323–330, [[hep-ph/0104277](#)].

[94] A. Banfi, G. Marchesini and G. Smye, *Away from jet energy flow*, *JHEP* **08** (2002) 006, [[hep-ph/0206076](#)].

[95] S. Caron-Huot, *Resummation of non-global logarithms and the BFKL equation*, *JHEP* **03** (2018) 036, [[1501.03754](#)].

[96] A. Banfi, F. A. Dreyer and P. F. Monni, *Higher-order non-global logarithms from jet calculus*, *JHEP* **03** (2022) 135, [[2111.02413](#)].

[97] A. Banfi, F. A. Dreyer and P. F. Monni, *Next-to-leading non-global logarithms in QCD*, *JHEP* **10** (2021) 006, [[2104.06416](#)].

[98] S. Ferrario Ravasio, K. Hamilton, A. Karlberg, G. P. Salam, L. Scyboz and G. Soyez, *Parton Showering with Higher Logarithmic Accuracy for Soft Emissions*, *Phys. Rev. Lett.* **131** (2023) 161906, [[2307.11142](#)].

[99] T. Becher, N. Schalch and X. Xu, *Resummation of Next-to-Leading Nonglobal Logarithms at the LHC*, *Phys. Rev. Lett.* **132** (2024) 081602, [[2307.02283](#)].

[100] J. R. Gaunt, *Glauber Gluons and Multiple Parton Interactions*, *JHEP* **07** (2014) 110, [[1405.2080](#)].

[101] M. Zeng, *Drell-Yan process with jet vetoes: breaking of generalized factorization*, *JHEP* **10** (2015) 189, [[1507.01652](#)].

[102] J. R. Forshaw and J. Holguin, *Coulomb gluons will generally destroy coherence*, *JHEP* **12** (2021) 084, [[2109.03665](#)].

[103] A. Banfi, J. R. Forshaw and J. Holguin, *The one-jettiness distribution contains super-super-leading logarithms*, [2511.11799](#).

[104] J. R. Forshaw, A. Kyrieleis and M. H. Seymour, *Super-leading logarithms in non-global observables in QCD*, *JHEP* **08** (2006) 059, [[hep-ph/0604094](#)].

[105] J. R. Forshaw, A. Kyrieleis and M. H. Seymour, *Super-leading logarithms in non-global observables in QCD: Colour basis independent calculation*, *JHEP* **09** (2008) 128, [[0808.1269](#)].

[106] J. Forshaw, J. Keates and S. Marzani, *Jet vetoing at the LHC*, *JHEP* **07** (2009) 023, [[0905.1350](#)].

[107] R. M. Duran Delgado, J. R. Forshaw, S. Marzani and M. H. Seymour, *The dijet cross section with a jet veto*, *JHEP* **08** (2011) 157, [[1107.2084](#)].

[108] T. Becher, M. Neubert and D. Y. Shao, *Resummation of Super-Leading Logarithms*, *Phys. Rev. Lett.* **127** (2021) 212002, [[2107.01212](#)].

[109] T. Becher, M. Neubert, D. Y. Shao and M. Stillger, *Factorization of non-global LHC observables and resummation of super-leading logarithms*, *JHEP* **12** (2023) 116, [[2307.06359](#)].

[110] P. Böer, M. Neubert and M. Stillger, *Glauber phases in non-global LHC observables: resummation for quark-initiated processes*, *JHEP* **10** (2023) 075, [[2307.11089](#)].

[111] P. Böer, P. Hager, M. Neubert, M. Stillger and X. Xu, *Glauber phases in non-global LHC observables: resummation for gluon-initiated processes*, *JHEP* **02** (2024) 109, [[2311.18811](#)].

[112] P. Böer, P. Hager, M. Neubert, M. Stillger and X. Xu, *Renormalization-group improved resummation of super-leading logarithms*, *JHEP* **08** (2024) 035, [[2405.05305](#)].

[113] T. Becher, P. Hager, G. Martinelli, M. Neubert, D. Schwienbacher and M. Stillger, *Super-leading logarithms in $pp \rightarrow 2$ jets*, *JHEP* **01** (2025) 171, [[2411.12742](#)].

[114] U. Banerjee, R. Grünhofer, M. König, Y. Li, M. Neubert and J. Scholze, *Super-Leading Logarithms in Top-Quark Pair Production at Hadron Colliders*, [2510.24848](#).

[115] M. Dasgupta, A. Fraley, P. F. Monni and S. Nabeebaccus, *Uncharted Logarithmic Structures in QCD Transverse-Energy Flow*, [2511.14681](#).

[116] S. Catani and M. H. Seymour, *A General algorithm for calculating jet cross-sections in NLO QCD*, *Nucl. Phys. B* **485** (1997) 291–419, [[hep-ph/9605323](#)].

[117] A. Karlberg, *disorder: Deep inelastic scattering at high orders*, *SciPost Phys. Codeb.* **2024** (2024) 32, [[2401.16964](#)].

[118] G. P. Salam and J. Rojo, *A Higher Order Perturbative Parton Evolution Toolkit (HOPPET)*, *Comput. Phys. Commun.* **180** (2009) 120–156, [[0804.3755](#)].

[119] M. Grazzini, S. Kallweit and M. Wiesemann, *Fully differential NNLO computations with MATRIX*, *Eur. Phys. J. C* **78** (2018) 537, [[1711.06631](#)].

[120] W. Bizoń, X. Chen, A. Gehrmann-De Ridder, T. Gehrmann, N. Glover, A. Huss et al., *Fiducial distributions in Higgs and Drell-Yan production at $N^3LL+NNLO$* , *JHEP* **12** (2018) 132, [[1805.05916](#)].

[121] J. Mazzitelli, P. F. Monni, P. Nason, E. Re, M. Wiesemann and G. Zanderighi, *Top-pair production at the LHC with MINNLO_{PS}*, *JHEP* **04** (2022) 079, [[2112.12135](#)].

[122] A. Banfi, G. P. Salam and G. Zanderighi, *NLL+NNLO predictions for jet-veto efficiencies in Higgs-boson and Drell-Yan production*, *JHEP* **06** (2012) 159, [[1203.5773](#)].

[123] J. Cruz-Martinez, S. Forte, N. Laurenti, T. R. Rabemananjara and J. Rojo, *LO, NLO, and NNLO parton distributions for LHC event generators*, *JHEP* **09** (2024) 088, [[2406.12961](#)].

[124] A. Karlberg, P. Nason, G. Salam, G. Zanderighi and F. Dreyer, *HOPPET v2.0.0 release note*, [2510.09310](#).

[125] A. Buckley, J. Ferrando, S. Lloyd, K. Nordström, B. Page, M. Rüfenacht et al., *LHAPDF6: parton density access in the LHC precision era*, *Eur. Phys. J. C* **75** (2015) 132, [[1412.7420](#)].

[126] C. Bierlich et al., *A comprehensive guide to the physics and usage of PYTHIA 8.3*, *SciPost Phys. Codeb.* **2022** (2022) 8, [[2203.11601](#)].

[127] M. Cacciari and G. P. Salam, *Pileup subtraction using jet areas*, *Phys. Lett. B* **659** (2008) 119–126, [[0707.1378](#)].

[128] M. Cacciari, G. P. Salam and G. Soyez, *The Catchment Area of Jets*, *JHEP* **04** (2008) 005, [[0802.1188](#)].

[129] G. Soyez, G. P. Salam, J. Kim, S. Dutta and M. Cacciari, *Pileup subtraction for jet shapes*, *Phys. Rev. Lett.* **110** (2013) 162001, [[1211.2811](#)].

[130] P. Berta, M. Spousta, D. W. Miller and R. Leitner, *Particle-level pileup subtraction for jets and jet shapes*, *JHEP* **06** (2014) 092, [[1403.3108](#)].

[131] M. Cacciari, G. P. Salam and G. Soyez, *SoftKiller, a particle-level pileup removal method*, *Eur. Phys. J. C* **75** (2015) 59, [[1407.0408](#)].

[132] D. Bertolini, P. Harris, M. Low and N. Tran, *Pileup Per Particle Identification*, *JHEP* **10** (2014) 059, [[1407.6013](#)].

[133] M. Cacciari, G. P. Salam and G. Soyez, *FastJet User Manual*, *Eur. Phys. J. C* **72** (2012) 1896, [[1111.6097](#)].

[134] M. van Beekveld, S. Ferrario Ravasio, A. Karlberg and N. Peake, “Generalised- k_t jet algorithms for Deep Inelastic Scattering,” In preparation.

[135] S. Abreu, J. R. Gaunt, P. F. Monni and R. Szafron, *The analytic two-loop soft function for leading-jet p_T* , *JHEP* **08** (2022) 268, [[2204.02987](https://arxiv.org/abs/2204.02987)].